REPORT DOCUMENTATION PAGE

Form Approved OMB NO. 0704-0188

1. REPORT DATE (DD-MM-YYYY)	2. REPORT TYPE	3. DATES COVERED (From - To)
16-07-2013	Final Report	15-Jun-2009 - 14-Jun-2013

4. TITLE AND SUBTITLE
Nonlinear Multiscale Modeling of 3D Woven Fiber Composites under Ballistic Loading

5a. CONTRACT NUMBER
W911NF-09-1-0210

5b. GRANT NUMBER

5c. PROGRAM ELEMENT NUMBER
611102

6. AUTHORS
Suvranu De

5d. PROJECT NUMBER

5e. TASK NUMBER

5f. WORK UNIT NUMBER

7. PERFORMING ORGANIZATION NAMES AND ADDRESSES
Rensselaer Polytechnic Institute
Office of Sponsored Research
Rensselaer Polytechnic Institute
Troy, NY 12180 -3522

8. PERFORMING ORGANIZATION REPORT NUMBER

9. SPONSORING/MONITORING AGENCY NAME(S) AND ADDRESS(ES)
U.S. Army Research Office
P.O. Box 12211
Research Triangle Park, NC 27709-2211

10. SPONSOR/MONITOR'S ACRONYM(S)
ARO

11. SPONSOR/MONITOR'S REPORT NUMBER(S)
54253-EG.23

12. DISTRIBUTION AVAILIBILITY STATEMENT
Approved for Public Release; Distribution Unlimited

13. SUPPLEMENTARY NOTES
The views, opinions and/or findings contained in this report are those of the author(s) and should not contrued as an official Department of the Army position, policy or decision, unless so designated by other documentation.

14. ABSTRACT
The objective of the current project is the development of the fundamentals of a novel two-scale multiscale computational method for the nonlinear damage and failure analysis of 3D woven fiber composites under ballistic loading. Since material behavior is determined by its microstructure, it is essential to accurately model the physics at that scale. The macroscale analysis provides a useful insight into the underlying high strain rate physics which is essential in modeling the lower micro-scale. In particular a rate dependent constitutive approach is being developed

15. SUBJECT TERMS
High strain rate loading, damage mechanics, 3D woven fiber composites, ballistic impact, multiscale modeling

16. SECURITY CLASSIFICATION OF:			17. LIMITATION OF ABSTRACT	15. NUMBER OF PAGES	19a. NAME OF RESPONSIBLE PERSON
a. REPORT	b. ABSTRACT	c. THIS PAGE			Suvranu De
UU	UU	UU	UU		19b. TELEPHONE NUMBER: 518-276-6096

Report Title

Nonlinear Multiscale Modeling of 3D Woven Fiber Composites under Ballistic Loading

ABSTRACT

The objective of the current project is the development of the fundamentals of a novel two-scale multiscale computational method for the nonlinear damage and failure analysis of 3D woven fiber composites under ballistic loading. Since material behavior is determined by its microstructure, it is essential to accurately model the physics at that scale. The macroscale analysis provides a useful insight into the underlying high strain rate physics which is essential in modeling the lower micro-scale. In particular a rate dependent constitutive approach is being developed coupled with continuum damage mechanics suitable for polymer materials. The effect of contact parameters on the underlying damage processes is being studied and worked on. We further develop a material model suitable particularly for loading of composites in the high strain rate regime. This is a significant development from the previous model where strain rate sensitivity is a-priori postulated for the matrix dominated modes in the small strain framework. We focused on developing a general homogenized anisotropic material model and obtained results which can be implemented in a finite element framework for high strain rate loading.

Enter List of papers submitted or published that acknowledge ARO support from the start of the project to the date of this printing. List the papers, including journal references, in the following categories:

(a) Papers published in peer-reviewed journals (N/A for none)

Received		Paper
07/16/2013	22.00	Ranajay Ghosh, Suvranu De. Z-Fiber Influence on High Speed Penetration of 3D Orthogonal Woven Fiber Composites, Mechanics of Materials, (07 2013): 0. doi:
08/19/2011	9.00	Suvranu De, Rahul. An efficient block preconditioner for Jacobian-free global-local multiscale methods, International Journal for Numerical Methods in Engineering, (08 2011): 0. doi: 10.1002/nme.3123
TOTAL:	**2**	

Number of Papers published in peer-reviewed journals:

(b) Papers published in non-peer-reviewed journals (N/A for none)

Received		Paper
TOTAL:		

Number of Papers published in non peer-reviewed journals:

(c) Presentations

Number of Presentations: 4.00

Non Peer-Reviewed Conference Proceeding publications (other than abstracts):

Received	Paper

TOTAL:

Number of Non Peer-Reviewed Conference Proceeding publications (other than abstracts):

Peer-Reviewed Conference Proceeding publications (other than abstracts):

Received	Paper	
08/18/2011	1.00	Suvranu De, Ranajay Ghosh. Progressive Damage Modeling of 3D Woven Fiber Composites under Ballistic Loading, Proceedings of the Society for the Advancement of Material and Process Engineering. 2011/05/23 00:00:00, . : ,

TOTAL: **1**

Number of Peer-Reviewed Conference Proceeding publications (other than abstracts):

(d) Manuscripts

Received		Paper
07/16/2013	17.00	Rahul, Suvranu De. Development of a Jacobian-free multiscale method (JFMM) with application to polycrystalline material modeling, Computer Methods in Applied Mechanics and Engineering (11 2012)
07/16/2013	19.00	Rahul, Suvranu De. Multiscale modeling of irradiated polycrystalline FCC metals, International Journal of Solids and Structures (03 2013)
07/16/2013	18.00	Amir R. Zamiri, Rahul, Suvranu De. A fully anisotropic single crystal model for high strain rate loading conditions with an application to ?-RDX, Journal of the Mechanics and Physics of Solids (11 2012)
08/22/2012	11.00	Rahul , Suvranu De. Jacobian-free multiscale method (JFMM): applied to neutron-irradiated polycrystalline metals, Journal of Computational Physics (09 2012)
08/22/2012	12.00	Rahul , Suvranu De. Jacobian-free multiscale method (JFMM): applied to polycrystalline material modeling, Computer Methods in Applied Mechanics and Engineering (09 2012)
08/22/2012	14.00	Ranajay Ghosh, Suvranu De. A Meso Scale Analysis of Ballistic Penetration of 3D Orthogonal Woven Fiber Composites, Mechanics of Materials (10 2011)
TOTAL:	**6**	

Number of Manuscripts:

Books

Received		Paper
09/07/2011	6.00	Suvranu De, Rahul. Recent Advances in Global-Local Multiscale Methods for Computational Mechanics, United Kingdom: Saxe-Coburg Publications, (10 2010)
TOTAL:	**1**	

Patents Submitted

Patents Awarded

Awards

Rahul is awarded US Association for Computational Mechanics (USACM) travel award for 12th US National Congress on Computational Mechanics, Raleigh, NC, 2013.

Graduate Students

NAME	PERCENT_SUPPORTED
FTE Equivalent:	
Total Number:	

Names of Post Doctorates

NAME	PERCENT_SUPPORTED
Rahul	0.60
FTE Equivalent:	**0.60**
Total Number:	**1**

Names of Faculty Supported

NAME	PERCENT_SUPPORTED	National Academy Member
Suvranu De	1.00	
FTE Equivalent:	**1.00**	
Total Number:	**1**	

Names of Under Graduate students supported

NAME	PERCENT_SUPPORTED
FTE Equivalent:	
Total Number:	

Student Metrics

This section only applies to graduating undergraduates supported by this agreement in this reporting period

The number of undergraduates funded by this agreement who graduated during this period:	0.00
The number of undergraduates funded by this agreement who graduated during this period with a degree in science, mathematics, engineering, or technology fields:.....	0.00
The number of undergraduates funded by your agreement who graduated during this period and will continue to pursue a graduate or Ph.D. degree in science, mathematics, engineering, or technology fields:.....	0.00
Number of graduating undergraduates who achieved a 3.5 GPA to 4.0 (4.0 max scale):	0.00
Number of graduating undergraduates funded by a DoD funded Center of Excellence grant for Education, Research and Engineering:	0.00
The number of undergraduates funded by your agreement who graduated during this period and intend to work for the Department of Defense	0.00
The number of undergraduates funded by your agreement who graduated during this period and will receive scholarships or fellowships for further studies in science, mathematics, engineering or technology fields:	0.00

Names of Personnel receiving masters degrees

NAME
Total Number:

Names of personnel receiving PHDs

NAME
Total Number:

Names of other research staff

NAME	PERCENT SUPPORTED
FTE Equivalent:	
Total Number:	

Sub Contractors (DD882)

Inventions (DD882)

Scientific Progress

"See Attachment"

Technology Transfer

Nonlinear Multiscale Modeling of 3D Woven Fiber Composites under Ballistic Loading

Final Report
Proposal Number: 54253EG

Suvranu De

July 11, 2013

Rensselaer Polytechnic Institute
110 8th Street, Troy, NY 12180 USA

Abstract

The objective of the current project is the development of the fundamentals of a novel two-scale multiscale computational method for the nonlinear damage and failure analysis of 3D woven fiber composites under ballistic loading. Since material behavior is determined by its microstructure, it is essential to accurately model the physics at that scale. The macroscale analysis provides a useful insight into the underlying high strain rate physics which is essential in modeling the lower micro-scale. In particular a rate dependent constitutive approach is being developed coupled with continuum damage mechanics suitable for polymer materials. The effect of contact parameters on the underlying damage processes is being studied and worked on. We further develop a material model suitable particularly for loading of composites in the high strain rate regime. This is a significant development from the previous model where strain rate sensitivity is *a-priori* postulated for the matrix dominated modes in the small strain framework. We focused on developing a general homogenized anisotropic material model and obtained results which can be implemented in a finite element framework for high strain rate loading.

Contents

List of Figures

List of Tables

1. Introduction

Ballistic penetration of composites involves a number of nonlinearities acting together stemming from high strain rates, contact-impact and evolving damage. The membrane models (Leigh Phoenix and Porwal 2003; Nadler et al. 2006), usually developed for fabric systems, are inapplicable in the case of 3D orthogonal woven composites (3D-OWC) because of elastic membrane assumptions, inability to incorporate strain rate effects, limitations pertaining to simple stress/strain based failure laws and lack of systematic framework to complicated geometries and large deformations. This limits the usability of these models for advanced composites like 3D-OWC. On the other hand, a microscale simulation with resolution of individual fiber filament is impractical due to enormous computational resources needed. This has led to various homogenization schemes both for material properties and damage laws. These methods increasingly popular since the middle of the last decade have severe technical difficulties. Some of these methods try to drastically cut computing time by unit cell level homogenization (Baheieldin et al. 2004; Bahei-El-Din and Zikry 2003; Pankow et al. 2011; Pankow et al. 2011). The periodicity of the unit cell makes it an ideal candidate for the classical representative volume element (RVE). However, this assumption is invalid for short wavelength regimes such as a pulse-loading event like ballistic impact. Oskay and Fish (2007) sidestep the problem by applying asymptotic homogenization at the level of fiber and filament through an eigendeformation formulation. Unfortunately their analysis neglects strain rate and material nonlinearities in addition to requiring, often intractable, mathematical manipulations. In addition,

using the fiber filament and surrounding matrix as RVE is questionable since the architecture of an actual 3D-OWC is far more complex. It must also be noted that most of damage laws have not been compared with experimental penetration events.

This issue is recently addressed by Sun et al. (2009) and Jia et al. (2010). A finite element analysis is performed with a critical damage area (CDA) theory at the unit cell level and results are compared with their own experiments. Although reasonable match between experimental and predicted exit velocities were reported, many of the material and damage parameters were taken *ad hoc* without a physical explanation. We would like to point out that developing models with a large number of parameters fit to match exit velocities only is not a viable modeling strategy due to its sensitivity to mesh distortion parameters, element deletion and the accuracy of the contact-impact conditions. In addition, obtaining exact dynamic material parameters for every mechanical phenomena proposed in the model would require enormous amount of testing and calibration. In the current work we address many of these shortcomings. We incorporate the nonlinearities in a systematic manner employing fewer parameters which can be independently obtained from experimentation of constituents of the composite. In addition, we employ a damage model which contains fewer parameters whose effects on the constitutive response are easier to understand and calibrate, are more intuitive to use and capture the physical consequences of the various damage modes.

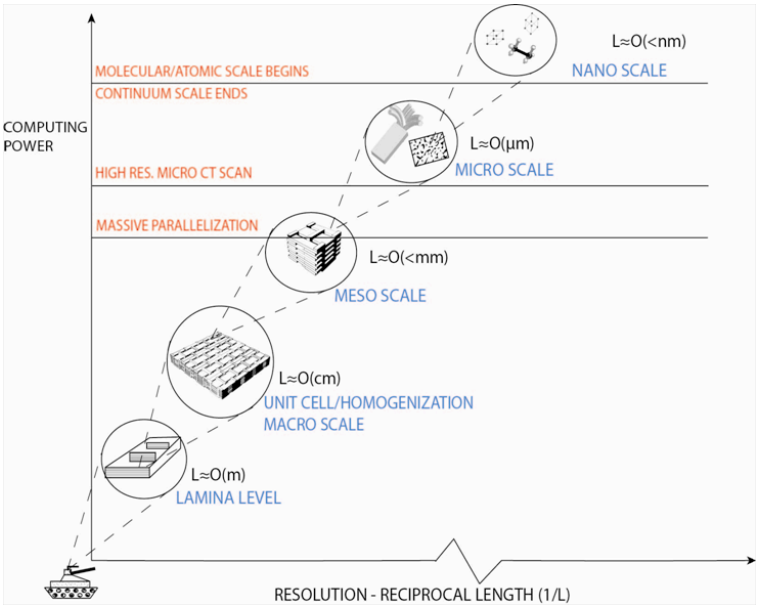

Figure 1: Spatial hierarchichal scales in a typical 3D-OWC applications.

Constitutive performance of heterogeneous solids cannot be accurately predicted if the effect of microstructure is not incorporated into the constitutive model. Micro structural effects are pronounced in composite materials because of the presence of many different constituents with widely different properties. Such a varied composition is useful to impart desirable properties

like high strength to weight ratio and resistance to impact damage. However, the variation of microstructure exists at various length scales, see Figure 1.

It is very clear that computational load steadily increases as we move up spatial resolution. Within the broad division of atomic and continuum scales their lie a number of length scales. We will like to point out that the resolution necessary to obtain a reasonably accurate response is greatly influenced by the loading of the structure. As the impact energy increases, the resolution needed to accurately capture the response drops sharply. This is primarily due to the appearance of distributed micro scale damage as well as short wavelength waves which can be smaller than the RVE of the medium. Therefore, it is inevitable that as the loading becomes more severe, for the same time period of computation, the computing requirement greatly increases forcing us to make an appropriate choice of the length scales. We characterize the scale that lies between the unit cells (cm) to the fiber filament level (μm) as the meso scale. We use this scale to split the sources of nonlinearities – inelasticity and damage in a systematic manner which is both simple as well as deals with lesser number of parameters. We exploit two simple characteristics of 3D-OWC – (1) delamination mode of damage is suppressed for localized loading due to 3D integral weave in one layer of 3D-OWC and (2) closely clustered resin impregnated fibers (henceforth we call it yarns) can be modeled separately from the resin rich regions and assumed to be solely responsible for damage accumulation through various anisotropic failure modes due to weak interfaces and stress concentrators. This meso level scale separation reduces computing costs greatly, obviates the theoretical problems with conventional multiscale methods and helps to systematically deal with nonlinearities according to the physics of the separated regions.

We develop a partitioned meso scale model for high strain rate modeling of ballistic impact on three-dimensional orthogonal woven composite. In this model, the entire material nonlinearity stemming from large deformation and strain rate effects before damage initiation was borne out by the polymeric resin. The anisotropic yarns are modeled using extensions of quasi-static small strain models with strain rate sensitivity empirically appended. We further extended the model of the yarn into a large deformation model.

Modeling of large strain mechanics has been attempted before for anisotropic composites (Simo 1987, Matzenmiller 1995). However, they have not been extended systematically for high strain rate loading of anisotropic composites where important material parameter like Gruneisen tensor and damage modes becomes dominant (Anderson et al. 1990, 1994). We propose a damage law based on consistent thermomechanics for a typical unidirectional composite, which can be easily extended for composites with greater degree of anisotropy.

The report is organized as follows. In section 2 we provide the details of the micromechanical constitutive model of resin. In section 3 constitutive and damage model for yarn is outlined. In section 4 the yarn model is further extended to accommodate finite deformation along with a yarn level damage model for high strain rate loading. In section 5 we discuss the simulation results followed by conclusions in section 6.

2. Constitutive modeling of resin

The polymer resin considered in the current model is epoxy which is well known to exhibit strong rate dependence (Jordan et al. 2008), not considered in detail in any previous model for ballistic penetration of 3D-OWC. We have adopted the large deformation, high strain rate model developed by Mulliken and Boyce (2006). The Mulliken-Boyce model assumes that the resistance to the deformation in thermoplastics is caused due to intermolecular resistance to chain segment rotation and an entropic resistance to chain alignment. The constitutive model decomposes intermolecular deformation resistance into contributions from primary 'α' processes and secondary 'β' processes. The α process is associated with rotations of the polymer main-chain segments and the β process is associated with restricted rotation of side groups. The model assumes that the material response may be approximated as simple superpositioning of the two. The model may be envisioned as a five component structure composed of a pair of linear elastic springs and viscoplastic dashpots '$A\alpha$' and '$A\beta$' corresponding to the α and β processes and a nonlinear Langevin spring 'B' acting in parallel. The basic kinematic assumptions are based on multiplicative Lee-Kroner decomposition of deformation gradient tensor '$\boldsymbol{F}$' applied to all,

$$\boldsymbol{F}_{A\alpha} = \boldsymbol{F}^{e}_{A\alpha}\boldsymbol{F}^{p}_{A\alpha}, \quad \boldsymbol{F}_{A\beta} = \boldsymbol{F}^{e}_{A\beta}\boldsymbol{F}^{p}_{A\beta}, \quad \det(\boldsymbol{F}^{p}_{A\alpha}) = \det(\boldsymbol{F}^{p}_{A\beta}) = 1 \tag{2.1}$$

followed by an additive split of the velocity gradient tensor as,

$$\boldsymbol{L}_{A\alpha} = \boldsymbol{L}^{e}_{A\alpha} + \boldsymbol{F}^{p}_{A\alpha}\boldsymbol{L}^{p}_{A\alpha}\boldsymbol{F}^{e-1}_{A\alpha} = \boldsymbol{L}^{e}_{A\alpha} + \tilde{\boldsymbol{L}}^{p}_{A\alpha}, \quad \boldsymbol{L}_{A\beta} = \boldsymbol{L}^{e}_{A\beta} + \boldsymbol{F}^{p}_{A\beta}\boldsymbol{L}^{p}_{A\beta}\boldsymbol{F}^{e-1}_{A\beta} = \boldsymbol{L}^{e}_{A\beta} + \tilde{\boldsymbol{L}}^{p}_{A\beta}. \tag{2.2}$$

The plastic velocity gradient is then additively decomposed into a symmetric stretch $(\tilde{\boldsymbol{D}}^{p}_{A\alpha}, \tilde{\boldsymbol{D}}^{p}_{A\beta})$ and an unsymmetrical rotational $(\tilde{\boldsymbol{W}}^{p}_{A\alpha}, \tilde{\boldsymbol{W}}^{p}_{A\beta})$ component. The later is equated to zero by the hypothesis of irrotational plasticity. The stretch is further described using a coaxial flow rule

$$\tilde{\boldsymbol{D}}^{p}_{A\alpha} = \dot{\gamma}^{p}_{i}\boldsymbol{N}^{p}_{Ai}, \quad \boldsymbol{N}^{p}_{Ai} = \frac{\boldsymbol{T}'_{Ai}}{\left|\boldsymbol{T}'_{Ai}\right|}, \quad i = \alpha, \beta \tag{2.3}$$

where primes denote deviatoric components of the Cauchy stress '$\boldsymbol{T}$' and $\dot{\gamma}^{p}_{i}$ the shear strain rate which is given by,

$$\dot{\gamma}^{p}_{i} = \dot{\gamma}^{p}_{0,i}\exp\left[-\frac{\Delta G_i}{k_B T}\left(1 - \frac{\tau_i}{s_i + \alpha_{p,i}p}\right)\right] \tag{2.4}$$

such that, $\tau_i = \left(\frac{1}{2}\boldsymbol{T}'_{Ai}\boldsymbol{T}'_{Ai}\right)^{1/2}$, $s_{0,i} = 0.077\frac{\mu_i}{(1-\nu_i)}$, and $\dot{s}_i = h_i\left(1 - \frac{s_i}{(1-s_{ss,i})}\right)\dot{\gamma}^{p}_{i}$; where $\dot{\gamma}^{p}_{0,i}$ is the pre-exponential factor, ΔG_i is the activation energy, k_B is the Boltzmann constant, T is the temperature, $\alpha_{p,i}$ is the pressure coefficient, p is the pressure, h_i is the softening slope, and s_i is the athermal shear strength representing the internal structure of the material and is related to

shear modulus μ_i and Poisson's ratio ν_i of the i^{th} component through an appropriate hardening law. The dependence of internal structure on shear strain rate is a significant conclusion especially during loading and unloading of waves and this effect cannot be captured by commonly used simple shear strain dependent stress-strain laws (Meyers 1994). The stress in the non-linear hardening component, the network "back stress" due to the entropic resistance to molecular alignment, is taken to be deviatoric and is computed as,

$$\boldsymbol{T}_B = \frac{C_R}{3}\frac{\sqrt{N}}{\lambda^p_{chain}} L^{-1}\left(\frac{\lambda^p_{chain}}{\sqrt{N}}\right)\bar{B}'_B \tag{2.5}$$

where $\lambda^p_{chain} = \sqrt{\dfrac{trace(\bar{B}_B)}{3}}$ is the stretch on a chain in the eight chain network, 'L' is the Langevin function defined by $L(\beta) = \coth\beta - \dfrac{1}{\beta}$, $\bar{B}'_B$ is the deviatoric part of the isochoric left Cauchy-Green tensor, $\bar{B}_B = (\det \boldsymbol{F}_B)^{-2/3}\boldsymbol{F}_B\boldsymbol{F}_B^T$, $\sqrt{N}$ is the limiting chain extensibility and $C_R = Nk\theta$ is the rubbery modulus and N is the number of chains per unit volume, k is the Boltzmann constant, and θ is the absolute temperature. The total stress in the polymer is given as the tensorial sum of the α and β intermolecular stresses and the network (back) stress, that is, $\boldsymbol{T} = \boldsymbol{T}_{A\alpha} + \boldsymbol{T}_{A\beta} + T_B$. Here, we simplify the composite failure by proposing a terminal failure model for the bulk matrix and account for the damage accumulation in the failure of the anisotropic fiber yarn. The bulk matrix polymer resin is assumed to fail terminally when failure strain is reached. This can be expressed in terms of the molecular chain stretch λ^p_{chain} as,

$$\lambda^p_{chain} \geq \lambda^p_{chain,cr}, \quad T \geq T_{cr}, \quad \sigma_{ij} = 0\,. \tag{2.6}$$

Here $\lambda^p_{chain,cr}$ is critical molecular chain length extension T_{cr} is the melting temperature and σ_{ij} is internal Cauchy stress. Bergstrom et al. (2005) have demonstrated that this molecular chain length failure criterion is far more consistent than strain envelopes for polymers. In addition, the terminal damage law automatically takes into account the ductile to brittle transition at high strain rates.

The resin is assumed to be Epon epoxy and its properties are taken from a recent paper by Jordan et al. (2008) and reproduced here. Since adiabatic conditions are usually assumed during a typical high strain rate events, local rise of temperature can be computed without taking recourse to solving a heat transfer problem. We note that conversion of dissipative work to heat is a rather complex process for polymers where only a fraction of post yield work is converted to heat with the rest being stored (Garg et al. 2008). In the current work, we assume that the dissipated work is contributed solely by the α and β component whereas the Langevin spring acts as pure energy storage component. If we denote the specific heat of epoxy as C_p and mass density as ρ we arrive at the following relation for rate of dissipated work (power),

$$\dot{W}^{diss} = \boldsymbol{T}_{A\alpha} : \tilde{\boldsymbol{D}}^{p}_{A\alpha} + \boldsymbol{T}_{A\beta} : \tilde{\boldsymbol{D}}^{p}_{A\beta} \tag{2.7}$$

where overhead dot indicates time derivative and colon indicates scalar product.

Assuming only a fraction β of this power is used to raise the temperature θ, we arrive at the following expression,

$$\dot{\theta} = \beta \frac{\dot{W}^{diss}}{\rho C_p} . \tag{2.8}$$

The exact value of the scalar β varies from 0.4 to 0.6 depending on strain and strain rates (Garg et al. 2008). In the current problem we assume the value of β=0.5.

Table 1: Parameters of the Mulliken-Boyce model for EPON Epoxy[1].

$\nu_\alpha(\theta,\dot{\varepsilon}),\ \nu_\beta(\theta,\dot{\varepsilon})$	0.38
$\dot{\gamma}_{0,\alpha}(\theta,\dot{\varepsilon})$	$2.29\times10^{15}s^{-1}$
$\dot{\gamma}_{0,\beta}(\theta,\dot{\varepsilon})$	$2.0\times10^{6}s^{-1}$
ΔG_α	$3.83\times10^{-19}J$
ΔG_β	$3.32\times10^{-20}J$
$\alpha_{p,\alpha},\ \alpha_{p,\beta}$	0.316
$s_{ss,\alpha},\ s_{ss,\beta}$	$0.58MPa$
$h_\alpha,\ h_\beta$	$300MPa$
C_R	$14.2MPa$
N	$2.3m^{-1/2}$
ρ	$1140Kg\ cm^{-3}$
C_P	$2000JKg^{-1}K^{-1}$

[1]Jordan et al. 2008

The strain rate dependent values of elastic constants are obtained from the DMA curves. The temperature rise predicted from the model can be seen in the Figure 2(a) and (b). It is clear from the figure that temperature rise can be significant and burning of epoxy is very likely since the ignition temperature of many epoxy derivatives are about 800K. This prediction is in agreement with the experimental findings of Walter et al. (2009) who have reported a distinct burning epoxy smell after the experiments. We will assume terminal damage of material occurs at the ignition point. Interestingly, dependence of temperature rise on shear strain indicates that beyond a certain point, a runaway softening is possible in the material. This kind of thermal instability has been reported by in 3D-OWC by Pankow et al. (2011) in their SHPB experiments. However, we would like to note that in an actual penetration event macroscopic shear bands which can form underneath a projectile are quickly interrupted by the penetrating projectile as well as other

failure modes brought about by rapid through thickness wave propagation making post impact data reduction difficult. The shear bands may indeed form at the edges of the projectile due to strain localization but macroscopic cracks are likely to be interrupted by the much stronger fibers present in all three directions within a unit cell. It also likely that localized micro bands can become the sites of void nucleation thus activating other modes of mechanical failure. Therefore, possibility of shear bands alone may not necessarily cause defeat of an actual armor.

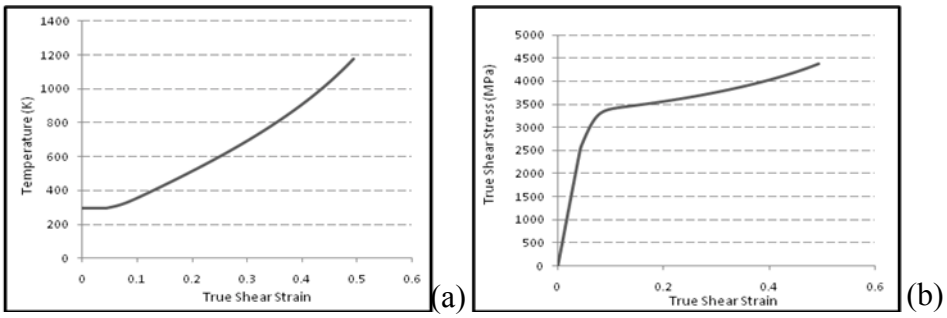

Figure 2: (a) Temperature vs true shear strain and (b) shear stress (Cauchy) vs true shear strain both at pure shear strain rate of 2×10^{6} s^{-1}.

3. Constitutive modeling of yarns

Next, we describe the response of the fibers. The fibers themselves are held together by the resin forming a composite yarn. There yarns are composed of individual fibers running axially, embedded in the surrounding matrix material. For most ballistic applications involving 3D composites, S2-glass fibers are commonly employed which can be treated as elastic brittle with negligible plastic zone. Moreover, the distribution of the fibers inside the yarn is assumed to be uniform for every cross section which allows us to consider them as transverse and isotropic. We assume no twisting of the yarn which is a characteristic of the most popular 3D-OWC produced by 3Tex® Inc. Hence, these yarns can be treated as unidirectional composite by themselves embedded in the larger 3D composite. It is well known that unidirectional laminates exhibit strong nonlinearities in shearing response (Hahn and Tsai 1973).However, since the impact process causes quick proliferation of defects and microcracks, all the nonlinearity is assumed to come from damage which will be modeled in the next section. In addition, the basic assumption of yarn being a homogenized continuum is assumed to be valid at the yarn level. This assumption is similar to the one used by Matzenmiller et al. (1995) and implies that the defects in the composite material are treated in the mathematical model as having the equivalent effect on the elastic properties as disk-like cracks would exert, if they are only oriented either tangential or normal to the fiber direction. The rate effects on elastic property is neglected since the rate effects on the pre-yield modulus is small as seen from the slopes of the stress strain curve of epoxy (Jordan et al. 2008).

For moderately high concentration, various closed form solutions have been provided for fiber composites using the generalized self consistent for fiber composites (Christensen 1990).

We use these closed form expressions for our current problem since they are simpler and easier to use for various material parameters compared to variational methods like Mori-Tanaka estimates (Nemat-Nasser 1993). We denote the fiber and matrix Young's modulus, shear modulus and Poisson ratio is denoted as E_f, ν_f, μ_f and E_m, ν_m, μ_m, respectively. These properties can be used to predict the five effective elastic properties of the transversely isotropic yarns – E_{11} the axial modulus, ν_{12} the axial Poisson's ratio, μ_{12} the axial shear modulus, K_{23} the plane strain bulk modulus and μ_{23} the transverse shear modulus, where $\boldsymbol{e}_1$ is the fiber direction. If we denote the fiber volume fraction as *c*, we arrive at the following expressions (Christensen 1990),

$$E_{11} = cE_f + (1-c)E_m + \frac{4c(1-c)(\nu_f - \nu_m)^2 \mu_m}{(1-c)\left(\frac{\mu_m}{k_f + \frac{1}{3}\mu_f}\right) + c\left(\frac{\mu_m}{k_m + \frac{1}{3}\mu_m}\right) + 1} \tag{3.1}$$

$$\nu_{12} = c\nu_f + (1-c)\nu_m + \frac{c(1-c)(\nu_f - \nu_m)\left(\frac{\mu_m}{k_m + \frac{1}{3}\mu_m} - \frac{\mu_m}{k_f + \frac{1}{3}\mu_f}\right)\mu_m}{(1-c)\left(\frac{\mu_m}{k_f + \frac{1}{3}\mu_f}\right) + c\left(\frac{\mu_m}{k_m + \frac{1}{3}\mu_m}\right) + 1} \tag{3.2}$$

$$\frac{\mu_{12}}{\mu_m} = \frac{\mu_f(1+c) + \mu_m(1-c)}{\mu_f(1-c) + \mu_m(1+c)} \tag{3.3}$$

$$K_{23} = k_m + \frac{1}{3}\mu_m + \frac{c}{\frac{1}{k_f - k_m + \frac{1}{3}(\mu_f - \mu_m)} + \frac{1-c}{k_m + \frac{4}{3}\mu_m}} \tag{3.4}$$

and μ_{23} is given by the following quadratic equation,

$$A\left(\frac{\mu_{23}}{\mu_m}\right)^2 + 2B\left(\frac{\mu_{23}}{\mu_m}\right) + C = 0 \tag{3.5}$$

where *A*, *B* and *C* are themselves functions of elastic properties of matrix and fibers and are given as,

$$\begin{aligned} A = {} & 3c(1-c)^2\left(\frac{\mu_f}{\mu_m} - 1\right)\left(\frac{\mu_f}{\mu_m} + \eta_f\right) \\ & + \left[\frac{\mu_f}{\mu_m}\eta_m + \eta_f\eta_m - \left(\frac{\mu_f}{\mu_m}\eta_m - \eta_f\right)c^3\right]\left[c\eta_m\left(\frac{\mu_f}{\mu_m} - 1\right) - \left(\frac{\mu_f}{\mu_m}\eta_m + 1\right)\right] \end{aligned} \tag{3.6}$$

$$
\begin{aligned}
B = & -3c(1-c)^2\left(\frac{\mu_f}{\mu_m}-1\right)\left(\frac{\mu_f}{\mu_m}+\eta_f\right)+\frac{1}{2}\left[\eta_m\frac{\mu_f}{\mu_m}+\left(\frac{\mu_f}{\mu_m}-1\right)c+1\right] \\
& \times\left[(\eta_m-1)\left(\frac{\mu_f}{\mu_m}+\eta_f\right)-2\left(\frac{\mu_f}{\mu_m}\eta_m-\eta_f\right)c^3\right] \\
& +\frac{c}{2}(\eta_m+1)\left(\frac{\mu_f}{\mu_m}-1\right)\left[\frac{\mu_f}{\mu_m}+\eta_f+\left(\frac{\mu_f}{\mu_m}\eta_m-\eta_f\right)c^3\right]
\end{aligned} \tag{3.7}
$$

$$
\begin{aligned}
C = & 3c(1-c)^2\left(\frac{\mu_f}{\mu_m}-1\right)\left(\frac{\mu_f}{\mu_m}+\eta_f\right) \\
& +\left[\eta_m\frac{\mu_f}{\mu_m}+\left(\frac{\mu_f}{\mu_m}-1\right)c+1\right]\left(\frac{\mu_f}{\mu_m}+\eta_f\right)+\left(\frac{\mu_f}{\mu_m}\eta_m-\eta_f\right)c^3
\end{aligned} \tag{3.8}
$$

where $\eta_f = 3-4\nu_f$ and $\eta_m = 3-4\nu_m$.

Assuming $E_f = 240GPa$, $\nu_f = 0.3$, $E_m = 2GPa$, $\nu_m = 0.45$, $c = 0.6$ and using the usual relationship between elastic constants we arrive at the values shown in Table 2.

Table 2: Effective property of anisotropic resin impregnated yarns

E_{11}	ν_{12}	μ_{12}	K_{23}	μ_{23}
114.83 *GPa*	0.31	2.68 *GPa*	17.16 *GPa*	3.77 *GPa*

3.1. Yarn damage mechanics

Predicting damage and progressive failure in composite materials under impact is an active area of research. The morphology of composite material induces damage accumulation before ultimate structural collapse. Hence brittle failure based criterion will not yield satisfactory results as nonlinearities induced by accumulation of damage would be stepped over. On the other hand, accounting for every crack and void nucleated during loading together with wave scattering and fiber-matrix interfacial failures through a numerical code requires the kind of resolution which is beyond the reach of current computing and imaging technology. Therefore purely computational approaches, e.g., Oskay and Fish (2007) and Belytschko et al. (2008) which need tracking of cracks explicitly with restrictions on periodicity are impractical for complex, dynamic loading of fiber reinforced composites.

The damage accumulation is assumed to be completely addressed by the failure of the yarn. Accumulating damage can be addressed through the framework of continuum damage mechanics (CDM). The CDM approach relies on introducing phenomenological 'internal variables' which can track the degradation of the material within the limits of homogenization. These variables although don't have a direct bearing to the micromechanics of crack and void growth must

adhere strictly to restrictions imposed by the laws of thermodynamics. A good introduction with many representative problems can be found in the book by Lemaître (2005).

Due to integrally woven geometry of the 3D-OWC and localized ballistic impact loading, we neglect delamination mode of damage for the current model (Greenhalgh 2009). The effect of friction is also neglected. The yarn failure is thus predominantly due to damage accumulation through the intralaminar damage modes. Neglecting delamination, we propose three damage scalars D_F, D_T and D_S associated with fiber breakage, transverse cracking and shear damage respectively. Under these assumptions, we can write the Gibbs free energy for the yarn as (Lemaître 2005),

$$G = \frac{\sigma_{11}^2}{2(1-D_F)E_1} + \frac{1}{2E_2}\left[\frac{\sigma_{22}^2}{(1-D_T)}\right] - \frac{1}{2}\left[\frac{\nu_{21}}{E_2} + \frac{\nu_{12}}{E_1}\right]\sigma_{11}\sigma_{22} + \frac{\sigma_{12}^2}{2(1-D_S)G_{12}} \tag{3.9}$$

Where σ_{ij} is the Cauchy stress, $\boldsymbol{e}_1$ is the fiber direction with transverse symmetry in the $\boldsymbol{e}_2 - \boldsymbol{e}_3$ plane, E_1 is the tensile Young's modulous, $E_2 = E_3$ is the transverse Young's modulous and G_{12} is the shear modulous. We can use the above expression of Gibbs free energy to obtain the compliance matrix *H* for the lamina,

$$\varepsilon_I = \frac{\partial G}{\partial \sigma_I} = [H]\{\sigma\} \tag{3.10}$$

where ε_I and σ_I are Cauchy stress components in Voigt notation. This leads to,

$$H_{IJ} = \frac{\partial^2 G}{\partial \sigma_I \partial \sigma_J} = \begin{bmatrix} \frac{1}{(1-D_F)E_1} & -\frac{1}{2}\left[\frac{\nu_{21}}{E_2} + \frac{\nu_{12}}{E_1}\right] & 0 \\ -\frac{1}{2}\left[\frac{\nu_{21}}{E_2} + \frac{\nu_{12}}{E_1}\right] & \frac{1}{(1-D_T)E_1} & 0 \\ 0 & 0 & \frac{1}{(1-D_S)E_1} \end{bmatrix} \tag{3.11}$$

The compliance clearly indicates that the damage variables are effectively degrading the stiffness of the matrix through the scalar damage parameters. However, it must be noted that damage caused by tension can be different from that caused by compression. To keep track of this variation, we rewrite the damage variables as,

$$\begin{aligned} D_F &= D_{F^+}\frac{\langle \sigma_{11} \rangle}{|\sigma_{11}|} + D_{F^-}\frac{\langle -\sigma_{11} \rangle}{|\sigma_{11}|} \\ D_T &= D_{T^+}\frac{\langle \sigma_{22} \rangle}{|\sigma_{22}|} + D_{T^-}\frac{\langle -\sigma_{22} \rangle}{|\sigma_{22}|} \end{aligned} \tag{3.12}$$

where $\langle x \rangle$ is the McCauley operator defined as $\langle x \rangle = (x + |x|)/2$. In this way, the eventual closure of transverse cracks under load reversal is taken into account. Depending on the sign of the corresponding normal stresses, a damage mode can be either active or passive. The model also assumes that the shear damage variable D_S is not affected by the closure effect. It should be noted that shear damage is caused mainly by transverse cracks which do not close under shear stresses. The stiffness degradation through damage evolution starts as soon as damage initiation conditions are met. The damage variables then evolve till a critical failure value is reached at which point the material is said to have failed and unable to resist any loading. In the current work, we assume that damage evolution rate depends on the current state of stress, strain and damage of that particular mode with no interactive modes. The damage initiation function is assumed to depend purely on stress. Mathematically we can write this as,

$$\dot{D}_\alpha = \begin{cases} 0, & f_\alpha(\boldsymbol{\sigma}) < f_{cr'} \\ \phi_\alpha(\boldsymbol{\sigma}, \dot{\boldsymbol{\varepsilon}}, D_\alpha), & f_\alpha(\boldsymbol{\sigma}) < f_{cr'} \end{cases} \qquad (3.13)$$
$$D_\alpha(\mathbf{0}) = 0, \quad \alpha = F^{\pm}, T^{\pm}, S$$

where α is the damage mode, f_α, and ϕ_α, is the damage initiation and damage evolution function associated with the α mode. The initiation and evolution functions represent various stages of crack and void growth and nucleation. In other words the evolution of D_α from 0 to a critical value $D_{\alpha,cr}$, represents proliferation of cracks and voids which continually degrade the stiffness, $C_{IJ} = [H]^{-1}$ from an initial value of C_{IJ}^0 to $\{0\}$ when all damage modes have reached their critical value and the material is assumed to fail completely. Unfortunately obtaining the initiation and evolution values from actual measurements of crack and void density, shape, size etc. is impossible and hence phenomenological relations are often postulated. There is no unanimity on the value of critical damage variable either. It represents the point beyond which steady macro cracks cause failure. An indirect way to obtain damage evolution and completion is using an energy release approach wherein energy released after critical damage has been released is equated with fracture energy experiments. In other words, the area under the stress-displacement curve after the initiation state is reached is obtained from experimental fracture energy experiments. Once a shape is postulated (which corresponds to the damage evolution law), one can precisely obtain the final displacement to failure. Pathological mesh dependency is eliminated by normalization through a characteristic length scale which depends on the mesh size. The critical damage variable when the material is failed is obtained when damage energy dissipation reaches the energy release rate obtained from fracture mechanics experiments. The physical basis of this theory closely follows the crack band theory developed by Bazant and Oh (1983) for concrete and is explained in detail in a recent paper by Lapczyk and Hurtado (2007). The Hashin-Rotem criterion (Hashin and Rotem 1973) is often used to initiate the damage modes in fiber reinforced composite. According to the criteria damage accumulation starts when scalar functions representing each failure mode - fiber tension (F_f^t), fiber compression (F_f^c), matrix

tension (F_m^t) and matrix compression (F_m^c) reach a critical value (in the current case=1). The expressions used are given in Table 3.

Table 3: Description of the Hashin-Rotem damage initiation model

Fiber Tension ($\sigma_{11} \geq 0$)	$F_f^t = \left(\frac{\sigma'_{11}}{X^T}\right)^2$
Fiber Compression ($\sigma_{11} \leq 0$)	$F_f^c = \left(\frac{\sigma'_{11}}{X^C}\right)^2$
Matrix Tension ($\sigma_{22} \geq 0$)	$F_m^t = \left(\frac{\sigma'_{22}}{Y^T}\right)^2$
Matrix Compression($\sigma_{22} \leq 0$)	$F_m^c = \left(\frac{\sigma'_{22}}{2S^T}\right)^2 + \left[\left(\frac{Y^C}{2S^T}\right)^2 - 1\right]\frac{\sigma'_{22}}{Y^C} + \left(\frac{\sigma'_{12}}{S^L}\right)^2$

X^T: longitudinal tensile strength, X^C: longitudinal compressive strength, Y^T: transverse tensile strength, Y^C: transverse compressive strength, S^L: longitudinal shear strength, S^T: longitudinal transverse strength, $\sigma' = H\varepsilon$, H is the instantaneous degraded compliance matrix and ε is strain in Voigt notation.

During ballistic loading however, dynamic conditions are present. However, since this failure model is used only for the yarn and S2 glass fibers exhibiting very little or no rate sensitivity, the matrix dominated transverse mode needs modification. It is well known that dynamic crack fracture is a complicated phenomenon where fracture energy depends on duration of loading, shear and longitudinal wave speeds as well as the possibility of crack branching. For the present case, we assume that loading takes place rather rapidly and as a first approximation the dynamic energy release rate is approximately 25% higher than the static case (Meyers 1994) for the matrix dominated transverse modes. We assume that transverse failure initiation values are very close to the yield strength of polymer matrix resin. Noting the yield strength increase of resin material with increasing strain rate (Mulliken and Boyce 2006), we propose the following rate dependent failure initiation model for the matrix dominated failure initiation values Y^T, Y^C and S^L,

$$S^L = S_0^L\left(1 + \Lambda_{S^L}\ln\frac{\dot{\varepsilon}}{\dot{\varepsilon}_0}\right), \quad Y^\alpha = Y_0^\alpha\left(1 + \Lambda_{Y^\alpha}\ln\frac{\dot{\varepsilon}}{\dot{\varepsilon}_0}\right), \quad \alpha = T, C \tag{3.14}$$

where Y_0^T, Y_0^C and S_0^L are respectively the reference transverse tension, transverse compression and longitudinal damage initiation strengths evaluated at strain rates $\dot{\varepsilon}_0$ and $\dot{\varepsilon}'_{ij}$ is the deviatoric part of strain rate tensor. The reference strain rate, $\dot{\varepsilon}_0$ is taken to be 0.001 (Jordan et al. 2008) and Λ_{Y^α}, $\alpha = T, C$ and Λ_{S^L} are pre-multiplying factor which indicates the degree of strain rate sensitivity for each mode. The functional form is similar to the one proposed by Boyce et al.

(1988) and is simplified for the triaxial loading conditions by assuming the effective strain rate which is defined as,

$$\dot{\varepsilon} = \sqrt{\frac{2}{3}\dot{\varepsilon}'_{ij}\dot{\varepsilon}'_{ij}} \tag{3.15}$$

Since no experimental data is available to precisely obtain the value of these pre-multipliers for 3D composites, we use the value of 1 noting from Jordan et al. (2008)'s uniaxial experiments that yield strength roughly doubles when strain rate increases by two orders of magnitude. However, experimental testing can be done to yield a more accurate value of this exponent. The failure initiation values used in this work are given in Table 4.

Table 4: Failure initiation values for anisotropic yarns.

X^T (MPa)	X^C (MPa)	Y_0^T (MPa)	Y_0^C (MPa)	S_0^L (MPa)
6000	8000	6000	300000	7000

Finding the compression fracture energy for the model remains a challenge because not many standardized tests have been done for various fiber-matrix combinations. The only tests available in literature which can be directly used for our damage model have been done by Pinho et al. (2006) using a compact tension and compact compression specimen for T300/Epoxy composite. We have adapted Pinho and coworker's fracture data and the experiments done by Parhizgar et al. (1982), using values from 0^o and 90^o in the fracture energy calculations of Pinho et al. (2006). Using these approximations we arrive at the following damage properties for the yarn (Table 5):

Table 5: Fracture energy released rate for various damage modes

$G_{ft,c}(N/mm)$ (Fiber-tension)	$G_{fc,c}(N/mm)$ (Fiber-compression)	$G_{mt,c}(N/mm)$ (Matrix-tension)	$G_{mc,c}(N/mm)$ (Matrix-compression)
91600	76000	26800	22200

4. Constitutive modeling of transversely isotropic yarns

Fibers themselves are held together by the resin forming a composite yarn. There yarns are composed of individual fibers running axially, embedded in the surrounding matrix material. For most ballistic applications involving 3D composites, S2-glass fibers are commonly employed which can be treated as elastic brittle with negligible plastic zone. Moreover, the distribution of the fibers inside the yarn is assumed to be uniform for every cross section which allows us to consider them as transverse and isotropic. We assume no twisting of the yarn which is a characteristic of the most popular 3D-OWC produced by 3Tex® Inc. Hence, these yarns can be treated as unidirectional composite by themselves embedded in the larger 3D composite.

The body starts from initial configuration $\mathbf{B_0}$ at temperature θ_0 and at the end of loading (lasting for time Δt) is at the new configuration $\mathbf{B}$ with the new temperature θ. We instead

envision the step through a couple of intermediate stress free states denoted by **B*** and **B**. There is no heat transfer to the surroundings from the body.

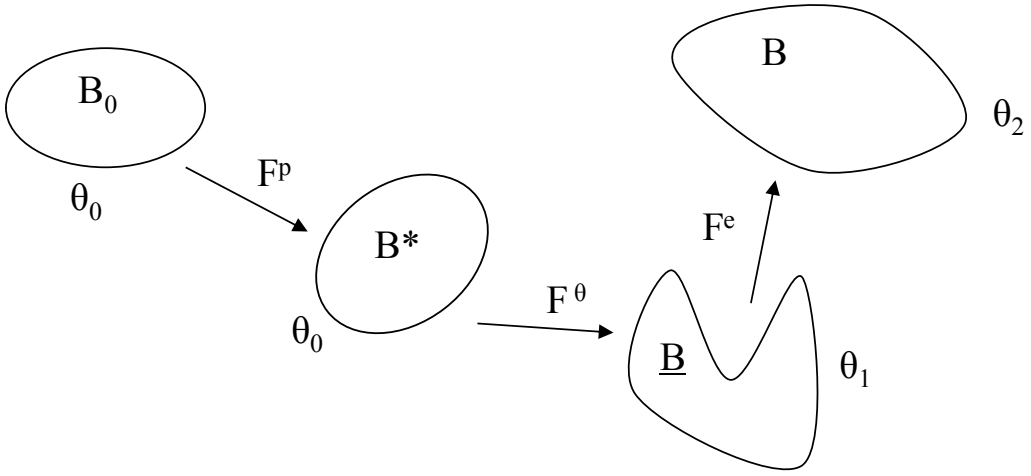

Figure 3: Decomposition of deformation through intermediate configuration.

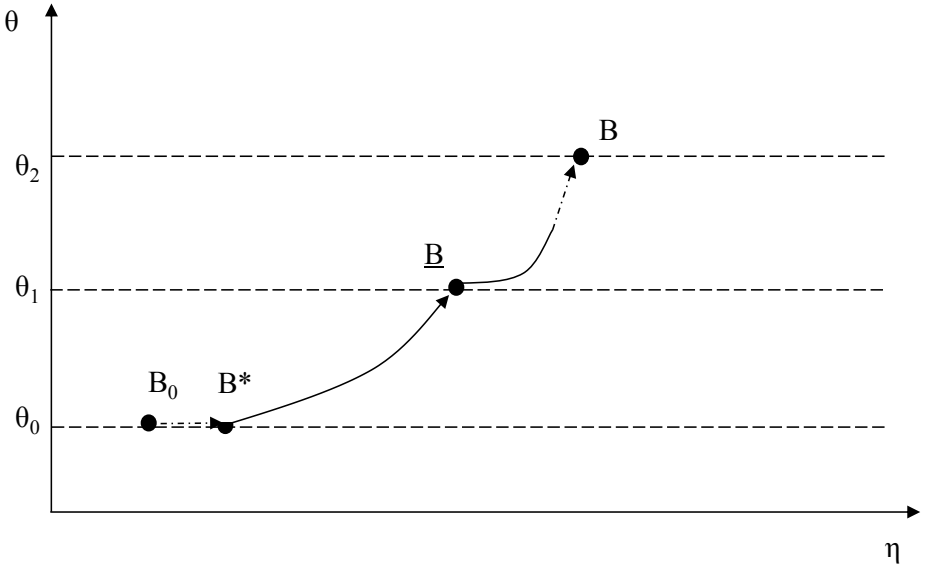

Figure 4: Intermediate decomposition on temperature-specific entropy diagram. Reversible processes are shown in solid arrows and irreversible processes in dashed lines.

The intermediate states can be described in a thermodynamic specific entropy (entropy per unit reference volume)-temperature (η-θ) diagram as show in Figure 2 below. From the picture it is clear that entropy is produced during the plastic step (**B_0-B***) due to various inelastic processes like motion of polymer chains, crack formation etc. We consider this entropy to be much smaller in comparison to other subsequent entropic processes. We consider the next thermal step (**B*-B**) to be reversible (equilibrium) and purely thermal taking the temperature from initial θ_0 to θ_1. The

heat transferred is supplied by the plastic dissipation from the previous plastic step (**B_0-B***). The next step (**B-B**) can be combination of reversible and irreversible step depending upon the presence of viscous effects.

4.1. Thermodynamics of intermediate steps

In this section, we look in detail, the thermodynamics of the intermediate steps.

*Step B_0-B**: This step is an isothermal, isochoric and adiabatic elastic unloading. The work in this step is used to create inelastic phenomena like dislocations, polymer chain sliding, cracking etc. The total work done is composed of elastic part and an inelastic part. The elastic part is assumed to increment (or decrease) the internal energy whereas part of the plastic part is assumed to produce heat.

Thus thermodynamically this can be written as:

$$\Delta e_{B_0-B^*} = -\delta w_{B_0-B^*} + \delta q_{B_0-B^*} + \delta \overline{q}_{B_0-B^*} \tag{4.1}$$

where Δe denotes internal energy change per unit initial (reference) volume, δw denotes specific work done by the system, δq denotes specific thermal heat added to/generated by the system, other irreversible sources such as acoustic/light etc are denoted by $\delta \overline{q}$ at this point. The total work during this elastic unloading can be divided into elastic and plastic work. The elastic work goes to change the internal energy and part of the plastic work causes heat production and other irreversible loss. Thus:

$$\Delta e_{B_0-B^*} = -\delta w^{el}_{B_0-B^*} - \delta w^{pl}_{B_0-B^*} + \delta q_{B_0-B^*} + \delta \overline{q}_{B_0-B^*} \tag{4.2}$$

If we assume that a certain fraction κ of plastic work goes directly to heat we have:

$$\delta q_{B_0-B^*} = \kappa\left(\delta w_{B_0-B^*}\right) = \kappa\left(\delta w^{pl}\right) \tag{4.3}$$

where δw^{pl} is the plastic work.

Step B-<u>B</u>*: In this step, the heat produced in the previous step causes internal energy change and no stress is applied to the system. Thus, it is a workless step. Reapplying the first law of thermodynamics once again, we have:

$$\Delta e_{B^*-\underline{B}} = -\delta w_{B^*-\underline{B}} + \delta q_{B^*-\underline{B}} + \delta \overline{q}_{B^*-\underline{B}} \tag{4.4}$$

Now $\delta w_{B^*-\underline{B}} = \delta \overline{q}_{B^*-\underline{B}} = 0$ due to purely thermal, stress free-state assumption. Assuming that the total thermal heat in step B_0-B* is applied during step B*-<u>B</u>, we have $\delta Q_{B^*-\underline{B}} = \delta Q_{B_0-B^*}$. Dividing throughout by reference volume $V_{B_0} = V_{B^*}$, we get $\delta q_{B^*-\underline{B}} = \delta q_{B_0-B^*}$. Thus, we have:

$$\Delta e_{B^*-\underline{B}} = \delta q_{B^*-\underline{B}} = \delta q_{B_0-B^*} = \kappa\left(\delta w^{pl}\right) \tag{4.5}$$

From basic thermodynamics, we have at constant stress:

$$\dot{q}_{B_0-B^*} = C_S\dot{\theta} = \kappa\dot{w}^{pl} \tag{4.6}$$

where C_S is the specific heat per unit reference volume and $\dot{w}^{pl}$ is the plastic power. Thus temperature equation can be written as:

$$\int_{\theta_0}^{\theta_1} C_S\, d\theta = \kappa\dot{w}^{pl}\Delta t \tag{4.7}$$

where Δt is the time increment. If specific heat per unit current volume is used, the thermal volume change must be taken into account.

4.2. Computing stress from elastic step

The elastic step consists of the process denoted by **B-B.** This can be reversible in the case of perfectly elastic material (which has no entropy sources) or partly irreversible in case of viscoelastic materials. This step can also be purely isothermal if elastic and viscous heating are completely neglected. We will proceed with each step relaxing the conditions on the way to derive the most general formulation. However, the thermomechanical building blocks are built here which would be applicable later.

We follow the standard *Coleman-Noll formulation* of extracting thermo-mechanical governing equations from the intrinsic dissipation inequality:

$$D_{int} = \frac{1}{2}\boldsymbol{S} : \dot{\boldsymbol{C}}^e - \dot{e} + \theta\dot{\eta} \geq 0 \tag{4.8}$$

where $\boldsymbol{S}$ is second Piola-Kirchoff stress and $\boldsymbol{C}^e$ is the elastic part of left Cauchy-Green stress, e and η are specific internal energy and specific entropy per unit referential volume, respectively, and θ is the temperature. If the process is purely reversible the equality holds or else the inequality.

It is clear from the above formulation that derivatives of energy and entropy must be calculated with respect to time. These time derivative are often converted to strain derivatives through chain rule. We carry out systematic analysis of these derivatives below.

We multiplicatively decompose the elastic deformation gradient as following:

$$\boldsymbol{F}^e = J_e^{1/3}\bar{\boldsymbol{F}}^e,\ \det(\bar{\boldsymbol{F}}^e) = 1 \tag{4.9}$$

Similarly, the left Cauchy-Green stress can be written as:

$$\boldsymbol{C}^e = \boldsymbol{F}^{eT}\boldsymbol{F}^e,\ \boldsymbol{C}^e = J_e^{2/3}\bar{\boldsymbol{C}}^e,\ \det(\bar{\boldsymbol{C}}^e) = 1 \tag{4.10}$$

This multiplicative split in the deformation gradient can be augmented by an additive split in the specific internal energy and specific entropy. For equilibrium processes (no viscoelasticity), this can be written as:

$$e\left(\theta,\boldsymbol{C}^e\right)=e_{vol}\left(\theta,J_e\right)+e_{iso}\left(\theta,\bar{\boldsymbol{C}}^e\right) \tag{4.11}$$

and

$$\eta\left(\theta,\boldsymbol{C}^e\right)=\eta_{vol}\left(\theta,J_e\right)+\eta_{iso}\left(\theta,\bar{\boldsymbol{C}}^e\right) \tag{4.12}$$

The energy derivatives can be written as following:

$$p_*=\left(\frac{\partial e_{vol}}{\partial J_e}\right)_\theta,\ \bar{\mathbf{S}}_*=2\left(\frac{\partial e_{iso}}{\partial \bar{\boldsymbol{C}}^e}\right)_\theta \tag{4.13}$$

It must be noted that p_* is not pressure (that would be derivative with respect to Helmholtz free energy at constant temperature). Similarly $\bar{\mathbf{S}}_*$ is not the usual isochoric stress.

The computation of entropic derivative is eased by the thermodynamic quantity called the Gruneisen tensor. The Gruneisen tensor is a thermodynamic measure of variation of entropy with strain and is a useful quantity in further derivation. This tensor's decomposition into volumetric and isochoric (deviatoric) parts will greatly aid in computation of time derivative of entropy which is an essential quantity for future derivations. The Gruneisen tensor is written as:

$$\boldsymbol{\Gamma}=\frac{2}{\mathrm{C}_{\mathrm{C}^e}}\left(\frac{\partial\eta}{\partial\boldsymbol{C}^e}\right)_\theta=\frac{2}{\mathrm{C}_{\mathrm{C}^e}}\left[\left(\frac{\partial\eta_{vol}(\theta,J_e)}{\partial\boldsymbol{C}^e}\right)_\theta+\left(\frac{\partial\eta_{iso}(\theta,\bar{\boldsymbol{C}}^e)}{\partial\boldsymbol{C}^e}\right)_\theta\right] \tag{4.14}$$

It can be shown that this tensor can be written as:

$$\boldsymbol{\Gamma}=\frac{2}{\mathrm{C}_{\mathrm{C}^e}}\left[\gamma\frac{J_e}{2}\boldsymbol{C}^{e-1}+J_e^{-2/3}\bar{\boldsymbol{\Gamma}}:\mathbf{P}^T\right] \tag{4.15}$$

where $\gamma=\frac{\partial\eta_{vol}}{\partial J_e}$, $\bar{\boldsymbol{\Gamma}}=\frac{\partial\eta_{iso}}{\partial\bar{\boldsymbol{C}}^e}$ and $\mathbf{P}^T=\mathbf{I}-\frac{1}{3}\boldsymbol{C}^{e-1}\otimes\boldsymbol{C}^e$ is the transpose of the projection tensor.

4.2.1. Purely elastic without structural heating

We are now in a position to compute the stress expressions. We start with the simplest case of isothermal purely-elastic step with no heating. In this case, the temperature in the step (**B**-**B**) remains constant at θ_1. The intrinsic dissipation for this step can be written as:

$$D_{int}=\frac{1}{2}\boldsymbol{S}:\dot{\boldsymbol{C}}^e-\dot{e}+\theta_1\dot{\eta} \tag{4.16}$$

This can be written using chain rule as:

$$D_{int}=\frac{1}{2}\boldsymbol{S}:\dot{\boldsymbol{C}}^e-\left(\frac{\partial e_{vol}}{\partial J_e}\dot{J}_e+\frac{\partial e_{iso}}{\partial\bar{\boldsymbol{C}}^e}:\dot{\bar{\boldsymbol{C}}}^e\right)+\theta_1\left(\frac{\partial\eta_{vol}}{\partial J_e}\dot{J}_e+\frac{\partial\eta_{iso}}{\partial\bar{\boldsymbol{C}}^e}:\dot{\bar{\boldsymbol{C}}}^e\right) \tag{4.17}$$

This can be recast as:

$$\begin{aligned} D_{int} &= \frac{1}{2}\boldsymbol{S}:\dot{\boldsymbol{C}}^e - \left(p_*\dot{J}_e + \bar{\mathbf{S}}_*:\frac{\dot{\bar{\boldsymbol{C}}}^e}{2}\right) + \theta_1\left(\gamma\dot{J}_e + \bar{\boldsymbol{\Gamma}}:\frac{\dot{\bar{\boldsymbol{C}}}^e}{2}\right) \\ &= \frac{1}{2}\boldsymbol{S}:\dot{\boldsymbol{C}}^e - \left(p_* - \gamma\theta_1\right)\dot{J}_e - \frac{1}{2}\left(\bar{\mathbf{S}}_*:\dot{\bar{\boldsymbol{C}}}^e + \theta\bar{\boldsymbol{\Gamma}}:\dot{\bar{\boldsymbol{C}}}^e\right) \end{aligned} \tag{4.18}$$

From tensor analysis we know:

$$\dot{J}_e = J_e\boldsymbol{C}^{e-1}:\frac{\dot{\boldsymbol{C}}^e}{2} \tag{4.19}$$

$$\dot{\bar{\boldsymbol{C}}}^e = 2J_e^{-\frac{2}{3}}\mathbf{P}^T:\frac{\dot{\boldsymbol{C}}^e}{2} \tag{4.20}$$

Thus we get the expression for intrinsic dissipation as:

$$\begin{aligned} D_{int} &= \frac{1}{2}\boldsymbol{S}:\dot{\boldsymbol{C}}^e - \left(p_* - \gamma\theta_1\right)J_e\boldsymbol{C}^{e-1}:\frac{\dot{\boldsymbol{C}}^e}{2} - J_e^{-\frac{2}{3}}\left(\bar{\mathbf{S}}_* - \theta\bar{\boldsymbol{\Gamma}}\right):\mathbf{P}^T:\frac{\dot{\boldsymbol{C}}^e}{2} \\ &= \left(\boldsymbol{S} - \left(p_* - \gamma\theta_1\right)J_e\boldsymbol{C}^{e-1} - J_e^{-\frac{2}{3}}\left(\bar{\mathbf{S}}_* - \theta_1\bar{\boldsymbol{\Gamma}}\right):\mathbf{P}^T\right):\frac{\dot{\boldsymbol{C}}^e}{2} \end{aligned} \tag{4.21}$$

Now due to perfect elasticity with no heating, the dissipation must disappear, leading to:

$$\boldsymbol{S} = \left(p_* - \gamma\theta_1\right)J_e\boldsymbol{C}^{e-1} - J_e^{-\frac{2}{3}}\left(\bar{\mathbf{S}}_* - \theta_1\bar{\boldsymbol{\Gamma}}\right):\mathbf{P}^T = \left(p - \gamma\theta_1\right)J_e\boldsymbol{C}^{e-1} - J_e^{-\frac{2}{3}}\mathbf{P}:\left(\bar{\mathbf{S}}_* - \theta_1\bar{\boldsymbol{\Gamma}}\right) \tag{4.22}$$

The conversion to Cauchy stress can be done using the following expression:

$$\boldsymbol{\sigma} = \frac{1}{J_e}\boldsymbol{F}^e\boldsymbol{S}\boldsymbol{F}^{eT} \tag{4.23}$$

or

$$\boldsymbol{\sigma} = \frac{1}{J_e}\left[\left(p_* - \gamma\theta_1\right)J_e\boldsymbol{F}^e\boldsymbol{C}^{e-1}\boldsymbol{F}^{eT} - J_e^{-\frac{2}{3}}\boldsymbol{F}^e\mathbf{P}:\left(\bar{\mathbf{S}}_* - \theta_1\bar{\boldsymbol{\Gamma}}\right)\boldsymbol{F}^{eT}\right] \tag{4.24}$$

Recalling the deviatoric-isochoric split of the deformation gradient, we arrive at:

$$\boldsymbol{\sigma} = \left(p_* - \gamma\theta_1\right)\boldsymbol{I} + J_e^{-1}\bar{\boldsymbol{F}}^e\left[\mathbf{P}:\left(\bar{\mathbf{S}}_* - \theta_1\bar{\boldsymbol{\Gamma}}\right)\right]\bar{\boldsymbol{F}}^{eT} \tag{4.25}$$

4.2.2. Purely elastic with structural heating

In the thermo-elastic step, there is temperature change. Thus the time rate of change of internal energy and entropy can be written as:

$$\dot{e}(\theta,\boldsymbol{C}^e)=\left(\frac{\partial e_{vol}(\theta,J_e)}{\partial J_e}\right)_\theta \dot{J}_e+\left(\frac{\partial e_{iso}(\theta,\bar{\boldsymbol{C}}^e)}{\partial \bar{\boldsymbol{C}}^e}\right)_\theta :\dot{\bar{\boldsymbol{C}}}^e+\left(\frac{\partial e}{\partial \theta}\right)_{\boldsymbol{C}^e}\dot{\theta} \tag{4.26}$$

and

$$\dot{\eta}(\theta,\boldsymbol{C}^e)=\left(\frac{\partial \eta_{vol}(\theta,J_e)}{\partial J_e}\right)_\theta \dot{J}_e+\left(\frac{\partial \eta_{iso}(\theta,\bar{\boldsymbol{C}}^e)}{\partial \bar{\boldsymbol{C}}^e}\right)_\theta :\dot{\bar{\boldsymbol{C}}}^e+\left(\frac{\partial \eta}{\partial \theta}\right)_{\boldsymbol{C}^e}\dot{\theta} \tag{4.27}$$

Thus, the intrinsic dissipation would become:

$$D_{int}=\frac{1}{2}\boldsymbol{S}:\dot{\boldsymbol{C}}^e-\left(p_*\dot{J}_e+\bar{\mathbf{S}}_*:\frac{\dot{\bar{\boldsymbol{C}}}^e}{2}+\left(\frac{\partial e}{\partial \theta}\right)_{\boldsymbol{C}^e}\dot{\theta}\right)+\theta\left(\gamma\dot{J}_e+\bar{\boldsymbol{\Gamma}}:\frac{\dot{\bar{\boldsymbol{C}}}^e}{2}+\left(\frac{\partial \eta}{\partial \theta}\right)_{\boldsymbol{C}^e}\dot{\theta}\right) \tag{4.28}$$

In other words:

$$D_{int}=\frac{1}{2}\boldsymbol{S}:\dot{\boldsymbol{C}}^e-\left(p_*\dot{J}_e+\bar{\mathbf{S}}_*:\frac{\dot{\bar{\boldsymbol{C}}}^e}{2}\right)+\theta\left(\gamma\dot{J}_e+\bar{\boldsymbol{\Gamma}}:\frac{\dot{\bar{\boldsymbol{C}}}^e}{2}\right)+\left(\theta\left(\frac{\partial \eta}{\partial \theta}\right)_{\boldsymbol{C}^e}-\left(\frac{\partial e}{\partial \theta}\right)_{\boldsymbol{C}^e}\right)\dot{\theta} \tag{4.29}$$

Clearly, the last term which is coefficient of temperature rate is identically zero from basic thermodynamics. Thus, the form of equation developed in the earlier section is preserved:

$$D_{int}=\frac{1}{2}\boldsymbol{S}:\dot{\boldsymbol{C}}^e-\left(p_*\dot{J}_e+\bar{\mathbf{S}}_*:\frac{\dot{\bar{\boldsymbol{C}}}^e}{2}\right)+\theta\left(\gamma\dot{J}_e+\bar{\boldsymbol{\Gamma}}:\frac{\dot{\bar{\boldsymbol{C}}}^e}{2}\right) \tag{4.30}$$

This is similar to previous section and thus yields the following Cauchy stress expression:

$$\boldsymbol{\sigma}=\left(p_*-\gamma\theta\right)\boldsymbol{I}+J_e^{-1}\bar{\boldsymbol{F}}^e\left[\mathbf{P}:\left(\bar{\mathbf{S}}_*-\theta\bar{\boldsymbol{\Gamma}}\right)\right]\bar{\boldsymbol{F}}^{eT} \tag{4.31}$$

However, an important distinction is that the temperature is no longer constant and its evolution with time must be separately provided for by a temperature evolution equation.

The temperature rise in this step is now a combination of both structural elastic as well as inelastic effects. The *temperature evolution* can be derived as follows:

$$\dot{\eta}(\boldsymbol{C}^e,\theta)=\frac{\partial \eta}{\partial \boldsymbol{C}^e}:\dot{\boldsymbol{C}}^e+\frac{\partial \eta}{\partial \theta}\dot{\theta} \tag{4.32}$$

We recall the following thermodynamic identities:

$$\boldsymbol{\Gamma}=\frac{2}{\mathrm{C}_{\mathrm{C}^e}}\left(\frac{\partial \eta}{\partial \boldsymbol{C}^e}\right)_\theta,\ \mathrm{C}_{\mathrm{C}^e}=\theta\left(\frac{\partial \eta}{\partial \theta}\right)_{\boldsymbol{C}^e} \tag{4.33}$$

Thus the above equation can be written as:

$$\dot{\eta}(\boldsymbol{C}^e,\theta) = \frac{C_{C^e}}{2}\boldsymbol{\Gamma} : \dot{\boldsymbol{C}}^e + \frac{C_{C^e}}{\theta}\dot{\theta} \tag{4.34}$$

This can be written as:

$$\theta\dot{\eta} = \frac{1}{2}\theta C_{C^e}\boldsymbol{\Gamma} : \dot{\boldsymbol{C}}^e + C_{C^e}\dot{\theta} \tag{4.35}$$

The heat transfer equation can next be written as:

$$\theta\dot{\eta} = -\nabla\cdot\boldsymbol{q} + D_{int} + R \tag{4.36}$$

where $\boldsymbol{q}$ is the heat flux, D_{int} is the internal dissipation and R is sum of local volumetric heat sources. Since the process is perfectly elastic and adiabatic, D_{int}=0, R=0, $\boldsymbol{q}$=$\boldsymbol{0}$. Thus eliminating entropy among the equations, we get:

$$0 = \frac{1}{2}\theta C_{C^e}\boldsymbol{\Gamma} : \dot{\boldsymbol{C}}^e + C_{C^e}\dot{\theta} \tag{4.37}$$

Thus, temperature evolution is given by:

$$\dot{\theta} = -\frac{1}{2}\theta\boldsymbol{\Gamma} : \dot{\boldsymbol{C}}^e \tag{4.38}$$

It can be shown that:

$$\dot{\theta} = -\theta\boldsymbol{\Gamma} : \boldsymbol{F}^{eT}\boldsymbol{D}^e\boldsymbol{F}^e \tag{4.39}$$

where $\boldsymbol{D}^e = \frac{1}{2}\left(\boldsymbol{L}^e + \boldsymbol{L}^{eT}\right)$ is the elastic stretch rate given in terms of the velocity gradient $\boldsymbol{L}^e$.

If the temperature at the end of this process is θ_2 the Cauchy-stress would be:

$$\boldsymbol{\sigma} = \left(p_* - \gamma\theta_2\right)\boldsymbol{I} + J_e^{-1}\bar{\boldsymbol{F}}^e\left[\mathbf{P} : \left(\bar{\mathbf{S}}_* - \theta_2\bar{\boldsymbol{\Gamma}}\right)\right]\bar{\boldsymbol{F}}^{eT} \tag{4.40}$$

4.2.3. Visco-elastic with structural heating/cooling

Viscoelastic phenomena is an inelastic phenomena which can occur even without a threshold effect. One way to model it is to assume viscoelasticity to come from purely non-equilibrium (NE) processes which is additive to the steady state internal energy and entropy through internal variables as:

$$e(\theta,\boldsymbol{C}^e,\xi_1) = e^{\infty}(\theta,\boldsymbol{C}^e) + e^{visc}(\theta,\xi_1,...,\xi_N) \tag{4.41}$$

$$\eta(\theta,\boldsymbol{C}^e,\xi_1) = \eta^{\infty}(\theta,\boldsymbol{C}^e) + \eta^{visc}(\theta,\xi_1,...,\xi_N) \tag{4.42}$$

where e^{∞} is the steady state response whereas e^{visc} is the non equilibrium response which is assumed to depend only on the deviatoric part of strain. Here, we would need an additional evolution equation for the internal variable is:

$$\dot{\xi}_{\alpha} = \dot{\xi}_{\alpha}(\xi_{\beta}, \bar{\boldsymbol{C}}^{e}),\ \alpha,\beta = 1...N \tag{4.43}$$

Writing the dissipation inequality:

$$D_{int} = \frac{1}{2}\boldsymbol{S} : \dot{\boldsymbol{C}}^{e} - \dot{e}(\theta, \boldsymbol{C}^{e}, \xi_1, ..., \xi_N) + \theta\dot{\eta}(\theta, \boldsymbol{C}^{e}, \xi_1, ..., \xi_N) \geq 0 \tag{4.44}$$

or

$$D_{int} = \frac{1}{2}\boldsymbol{S} : \dot{\boldsymbol{C}}^{e} - \dot{e}^{\infty}(\theta, \boldsymbol{C}^{e}) + \dot{e}^{visc}(\theta, \boldsymbol{C}^{e}, \xi_1, ..., \xi_N) + \theta\left[\dot{\eta}^{\infty}(\theta, \boldsymbol{C}^{e}) + \dot{\eta}^{visc}(\theta, \boldsymbol{C}^{e}, \xi_1, ..., \xi_N)\right] \geq 0 \tag{4.45}$$

where

$$\dot{e}^{visc}(\theta, \boldsymbol{C}^{e}, \xi_1, ..., \xi_N) = \sum \frac{\partial e^{visc}}{\partial \xi_{\alpha}} : \dot{\xi}_{\alpha} + \frac{\partial e^{visc}}{\partial \theta} : \dot{\theta} \tag{4.46}$$

Let us assume a simple evolution law:

$$\dot{\xi}_{\alpha} + \frac{\xi_{\alpha}}{\boldsymbol{\tau}_{\alpha}} = \beta_{\alpha}\dot{\bar{\boldsymbol{C}}}^{e} \tag{4.47}$$

plugging in above yields:

$$\dot{e}^{visc}(\theta, \boldsymbol{C}^{e}, \xi_1, ..., \xi_N) = \sum \frac{\partial e^{visc}}{\partial \xi_{\alpha}} : \left(\beta_{\alpha}\dot{\bar{\boldsymbol{C}}}^{e} - \frac{\xi_{\alpha}}{\boldsymbol{\tau}_{\alpha}}\right) + \frac{\partial e^{visc}}{\partial \theta} : \dot{\theta} \tag{4.48}$$

similarly:

$$\dot{\eta}^{visc}(\theta, \boldsymbol{C}^{e}, \xi_1, ..., \xi_N) = \sum \frac{\partial \eta^{visc}}{\partial \xi_{\alpha}} : \left(\beta_{\alpha}\dot{\bar{\boldsymbol{C}}}^{e} - \frac{\xi_{\alpha}}{\boldsymbol{\tau}_{\alpha}}\right) + \frac{\partial \eta^{visc}}{\partial \theta} : \dot{\theta} \tag{4.49}$$

Thus, the dissipation inequality becomes:

$$\begin{aligned} D_{int} = {} & \frac{1}{2}\boldsymbol{S} : \dot{\boldsymbol{C}}^{e} - \dot{e}^{\infty}(\theta, \boldsymbol{C}^{e}) + \theta\dot{\eta}^{\infty}(\theta, \boldsymbol{C}^{e}) - \sum \beta_{\alpha} \frac{\partial (e^{visc} - \theta\eta^{visc})}{\partial \xi_{\alpha}} : \dot{\bar{\boldsymbol{C}}}^{e} \\ & + \sum \frac{\partial (e^{visc} - \theta\eta^{visc})}{\partial \xi_{\alpha}} : \frac{\xi_{\alpha}}{\boldsymbol{\tau}_{\alpha}} \geq 0 \end{aligned} \tag{4.50}$$

Clearly the viscous terms multiplying the deviatoric strain rates have units of stress. In addition, recognizing the form of Helmholtz free energy, we get:

$$D_{int} = \frac{1}{2}\boldsymbol{S} : \dot{\boldsymbol{C}}^e - \dot{e}^{\infty}(\theta, \boldsymbol{C}^e) + \theta\dot{\eta}^{\infty}(\theta, \boldsymbol{C}^e) - \boldsymbol{S}^{visc} : \frac{\dot{\bar{\boldsymbol{C}}}_\alpha}{2} + \sum \frac{\partial \psi^{visc}}{\partial \xi_\alpha} : \frac{\xi_\alpha}{\tau_\alpha} \geq 0 \tag{4.51}$$

where

$$\boldsymbol{S}^{visc} = 2\sum \beta_\alpha \frac{\partial(e^{visc} - \theta\eta^{visc})}{\partial \xi_\alpha} = 2\sum \beta_\alpha \frac{\partial \psi^{visc}}{\partial \xi_\alpha} \tag{4.52}$$

assuming from construction of appropriate function the following is made to identically be satisfied $\sum \frac{\partial \psi^{visc}}{\partial \xi_\alpha} : \frac{\xi_\alpha}{\tau_\alpha} \geq 0$ and noting from equation (4.20), we get:

$$D_{int} = \frac{1}{2}\left(\boldsymbol{S} - J_e^{-\frac{2}{3}} \boldsymbol{S}^{visc} : \mathbf{P}^T \right) : \dot{\boldsymbol{C}}^e - \dot{e}^{\infty}(\theta, \boldsymbol{C}^e) + \theta\dot{\eta}^{\infty}(\theta, \boldsymbol{C}^e) \geq 0 \tag{4.53}$$

Now the above can be further simplified as:

$$D_{int} = \frac{1}{2}\hat{\boldsymbol{S}} : \dot{\boldsymbol{C}}^e - \dot{e}^{\infty}(\theta, \boldsymbol{C}^e) + \theta\dot{\eta}^{\infty}(\theta, \boldsymbol{C}^e) \geq 0, \quad \hat{\boldsymbol{S}} = \boldsymbol{S} - J_e^{-\frac{2}{3}} \boldsymbol{S}^{visc} : \mathbf{P}^T \tag{4.54}$$

This enormously simplifies our analysis for we can carry out our usual derivations for the remaining part thereby arriving at:

$$\hat{\boldsymbol{S}} = (p_*^{\infty} - \gamma\theta) J_e \boldsymbol{C}^{e-1} - J_e^{-\frac{2}{3}} (\bar{\mathbf{S}}_*^{\infty} - \theta\bar{\boldsymbol{\Gamma}}) : \mathbf{P}^T = (p_*^{\infty} - \gamma\theta) J_e \boldsymbol{C}^{e-1} - J_e^{-\frac{2}{3}} \mathbf{P} : (\bar{\mathbf{S}}_*^{\infty} - \theta\bar{\boldsymbol{\Gamma}}) \tag{4.55}$$

where $p_*^{\infty} = \frac{\partial e_{vol}^{\infty}(\theta, J_e)}{\partial J_e}$, $\bar{\mathbf{S}}_*^{\infty} = \frac{\partial e_{iso}^{\infty}(\theta, \bar{\boldsymbol{C}}_e)}{\partial \bar{\boldsymbol{C}}_e}$. The conversion to Cauchy stress can be done using equation (4.23) as follows:

$$\boldsymbol{\sigma} - \frac{1}{J_e}\boldsymbol{F}^e \left(J_e^{-\frac{2}{3}} \boldsymbol{S}^{visc} : \mathbf{P}^T \right) \boldsymbol{F}^{eT} = \left(p_* - \gamma\theta \right) \boldsymbol{I} + J_e^{-1} \bar{\boldsymbol{F}}^e \left[\mathbf{P} : \left(\bar{\mathbf{S}}_* - \theta\bar{\boldsymbol{\Gamma}} \right) \right] \bar{\boldsymbol{F}}^{eT} \tag{4.56}$$

or

$$\boldsymbol{\sigma} = \left(p_* - \gamma\theta \right) \boldsymbol{I} + J_e^{-1} \bar{\boldsymbol{F}}^e \left[\mathbf{P} : \left(\bar{\mathbf{S}}_* - \theta\bar{\boldsymbol{\Gamma}} + \boldsymbol{S}^{visc} \right) \right] \bar{\boldsymbol{F}}^{eT} \tag{4.57}$$

The temperature rise in this step is now a combination of both structural elastic as well as inelastic effects. The *temperature evolution* can be derived as follows:

$$\dot{\eta}(\theta, \boldsymbol{C}^e, \xi_1, ..., \xi_N) = \frac{\partial \eta}{\partial \boldsymbol{C}^e} : \dot{\boldsymbol{C}}^e + \frac{\partial \eta}{\partial \theta} : \dot{\theta} + \sum_{\alpha=1}^{N} \frac{\partial \eta}{\partial \xi_\alpha} : \dot{\xi}_\alpha \tag{4.58}$$

We recall the following $\boldsymbol{\Gamma} = \frac{2}{\mathrm{C}_{C^e}}\left(\frac{\partial \eta}{\partial \boldsymbol{C}^e}\right)_\theta$, $C_{C^e} = \theta\left(\frac{\partial \eta}{\partial \theta}\right)_{\boldsymbol{C}^e}$, $\frac{\partial \eta}{\partial \xi_\alpha} = \frac{\partial \eta^{visc}}{\partial \xi_\alpha}$; thus the above equation can be written as:

$$\dot{\eta}(\theta, \boldsymbol{C}^e, \xi_1, ..., \xi_N) = \frac{C_{C^e}}{2}\boldsymbol{\Gamma} : \dot{\boldsymbol{C}}^e + \frac{C_{C^e}}{\theta}\dot{\theta} + \sum_{\alpha=1}^{N} \frac{\partial \eta^{visc}}{\partial \xi_\alpha} : \dot{\xi}_\alpha \tag{4.59}$$

This can be written as:

$$\theta\dot{\eta} = \frac{1}{2}\theta \mathrm{C}_{C^e}\boldsymbol{\Gamma} : \dot{\boldsymbol{C}}^e + C_{C^e}\dot{\theta} + \theta\sum_{\alpha=1}^{N} \frac{\partial \eta^{visc}}{\partial \xi_\alpha} : \dot{\xi}_\alpha \tag{4.60}$$

The heat transfer equation can next be written as:

$$\theta\dot{\eta} = -\nabla \cdot \boldsymbol{q} + D_{int} + R \tag{4.61}$$

where $\boldsymbol{q}$ is the heat flux, D_{int} is the internal dissipation and R is sum of local volumetric heat sources. Since the process is adiabatic, $\boldsymbol{q}$=0. Thus eliminating entropy among the equations, we get:

$$D_{int} + R = \frac{1}{2}\theta \mathrm{C}_{C^e}\boldsymbol{\Gamma} : \dot{\boldsymbol{C}}^e + C_{C^e}\dot{\theta} + \theta\sum_{\alpha=1}^{N} \frac{\partial \eta^{visc}}{\partial \xi_\alpha} : \dot{\xi}_\alpha \tag{4.62}$$

Thus, temperature evolution is given by:

$$C_{C^e}\dot{\theta} = D_{int} + R - \frac{1}{2}\theta C_{C^e}\boldsymbol{\Gamma} : \dot{\boldsymbol{C}}^e - \theta\sum_{\alpha=1}^{N} \frac{\partial \eta^{visc}}{\partial \xi_\alpha} : \dot{\xi}_\alpha \tag{4.63}$$

Plugging in the value of intrinsic dissipation:

$$C_{C^e}\dot{\theta} = \left(\theta\sum_{\alpha=1}^{N} \frac{\partial \eta_\alpha^{visc}}{\partial \xi_\alpha} - \sum_{\alpha=1}^{N} \frac{\partial e_\alpha^{visc}}{\partial \xi_\alpha}\right) : \dot{\xi}_\alpha + R - \frac{1}{2}\theta C_{C^e}\boldsymbol{\Gamma} : \dot{\boldsymbol{C}}^e - \theta\sum_{\alpha=1}^{N} \frac{\partial \eta^{visc}}{\partial \xi_\alpha} : \dot{\xi}_\alpha$$

or (4.64)

$$C_{C^e}\dot{\theta} = R - \frac{1}{2}\theta C_{C^e}\boldsymbol{\Gamma} : \dot{\boldsymbol{C}}^e - \sum_{\alpha=1}^{N} \boldsymbol{\Xi}_\alpha : \dot{\xi}_\alpha$$

The temperature rise can be computed if the evolution equations for the internal variable are known:

$$\dot{\boldsymbol{\xi}}_\alpha = \dot{\boldsymbol{\xi}}_\alpha(\theta, \boldsymbol{C}^e, \boldsymbol{\xi}_1, ..., \boldsymbol{\xi}_K) \tag{4.65}$$

The final Cauchy stress then can be computed at final temperature θ_2 as:

$$\boldsymbol{\sigma} = \left(\tilde{p}_* - \tilde{\gamma}\theta_2\right)\boldsymbol{I} + J_e^{-1}\bar{\boldsymbol{F}}^e\left[\mathbf{P} : \left(\tilde{\bar{\mathbf{S}}}_* - \theta_2\tilde{\bar{\boldsymbol{\Gamma}}}\right)\right]\bar{\boldsymbol{F}}^{eT} \tag{4.66}$$

4.3. Fiber composite – hyperelastic case

Let us explore the case of fiber composite in detail. Let us denote the initial orientation of the fiber by the unit vector $\boldsymbol{a}_0$. Thus the internal energy can be written as:

$$e(\theta,\boldsymbol{C}^e) = e(\theta,\hat{\boldsymbol{a}}_0,\boldsymbol{C}^e) = e(\theta,I_1,I_2,I_3,I_4,I_5) = e(\theta,J_e,\bar{I}_1,\bar{I}_2,\bar{I}_4,\bar{I}_5) \tag{4.67}$$

where I_k and $\bar{I}_k$ are the strain invariants of the given problem and are given by:

$$I_1 = tr(\boldsymbol{C}^e), I_2 = \frac{1}{2}\left(I_1^2 - tr(\boldsymbol{C}^{e2})\right), I_3 = \det(\boldsymbol{C}^e), I_4 = \boldsymbol{a}_0 \cdot \boldsymbol{C}^e \boldsymbol{a}_0, I_5 = \boldsymbol{a}_0 \cdot \boldsymbol{C}^{e2} \boldsymbol{a}_0 \tag{4.68}$$

and

$$\bar{I}_1 = tr(\bar{\boldsymbol{C}}^e), \bar{I}_2 = \frac{1}{2}\left(\bar{I}_1^2 - tr(\bar{\boldsymbol{C}}^{e2})\right), \bar{I}_4 = \boldsymbol{a}_0 \cdot \bar{\boldsymbol{C}}^e \boldsymbol{a}_0, \bar{I}_5 = \boldsymbol{a}_0 \cdot \bar{\boldsymbol{C}}^{e2} \boldsymbol{a}_0 \tag{4.69}$$

Assuming a deviatoric/isochoric split in the energy:

$$e(\theta,J_e,\bar{I}_1,\bar{I}_2,\bar{I}_4,\bar{I}_5) = e_{vol}(\theta,J_e) + e_{iso}(\theta,\bar{I}_1,\bar{I}_2,\bar{I}_4,\bar{I}_5) \tag{4.70}$$

where

$$e_{vol}(\theta,J_e) = K(\theta)(J_e - 1)^2 \tag{4.71}$$

The fictitious modified isochoric stress $\bar{\mathbf{S}}_*$ can be written as:

$$\begin{aligned} \bar{\mathbf{S}}_* &= 2\frac{\partial e_{iso}}{\partial \bar{\mathbf{C}}} = 2\sum\nolimits_{\alpha=1,\alpha\neq 3}^{N} \frac{\partial e_{iso}}{\partial \bar{I}_\alpha} \cdot \frac{\partial \bar{I}_\alpha}{\partial \bar{\mathbf{C}}} \\ &= \bar{\gamma}_1 \boldsymbol{I} + \bar{\gamma}_2 \bar{\boldsymbol{C}} + \bar{\gamma}_4 \hat{\boldsymbol{a}}_0 \otimes \hat{\boldsymbol{a}}_0 + \bar{\gamma}_5 \left(\hat{\boldsymbol{a}}_0 \otimes \bar{\boldsymbol{C}}\hat{\boldsymbol{a}}_0 + \bar{\boldsymbol{C}}\hat{\boldsymbol{a}}_0 \otimes \hat{\boldsymbol{a}}_0\right) \end{aligned} \tag{4.72}$$

where $\bar{\gamma}_1 = 2\left(\frac{\partial e_{iso}}{\partial \bar{I}_1} + \bar{I}_1 \frac{\partial e_{iso}}{\partial \bar{I}_2}\right)$, $\bar{\gamma}_2 = -2\frac{\partial e_{iso}}{\partial \bar{I}_2}$, $\bar{\gamma}_4 = 2\frac{\partial e_{iso}}{\partial \bar{I}_4}$, $\bar{\gamma}_5 = 2\frac{\partial e_{iso}}{\partial \bar{I}_5}$

In indicial notation,

$$\begin{aligned} &\boldsymbol{X} = \hat{\boldsymbol{a}}_0 \otimes \bar{\boldsymbol{C}}\hat{\boldsymbol{a}}_0,\ X_{ij} = a_{0i}\bar{C}_{jk}a_{0k} = a_{0i}a_{0k}\bar{C}_{jk} \\ &\boldsymbol{X} = \hat{\boldsymbol{a}}_0 \bar{\boldsymbol{C}} \otimes \hat{\boldsymbol{a}}_0,\ X_{ij} = a_{0k}\bar{C}_{ki}a_{0j} = a_{0k}a_{0j}\bar{C}_{ki} \end{aligned} \tag{4.73}$$

Thus:

$$\bar{\mathbf{S}}_{*ij} = \bar{\gamma}_1 \delta_{ij} + \bar{\gamma}_2 \bar{C}_{ij} + \bar{\gamma}_4 a_{0i}a_{0j} + \bar{\gamma}_5 \left(a_{0i}a_{0k}\bar{C}_{jk} + a_{0k}a_{0j}\bar{C}_{ki}\right) \tag{4.74}$$

The anisotropic potential takes the following form (simple extension of Mooney-Rivlin):

$$e_{iso}(\theta,\bar{I}_1,\bar{I}_2,\bar{I}_4,\bar{I}_5) = \alpha_1(\theta)(\bar{I}_1 - 3) + \alpha_2(\theta)(\bar{I}_2 - 3) + \alpha_4(\theta)(\bar{I}_4 - 1) + \alpha_5(\theta)(\bar{I}_5 - 1) \tag{4.75}$$

Therefore,

$$\bar{\gamma}_1 = 2\Big(\alpha_1(\theta) + \bar{I}_1\,\alpha_2(\theta)\Big),\ \bar{\gamma}_2 = -2\alpha_2(\theta),\ \bar{\gamma}_4 = 2\alpha_4(\theta),\ \bar{\gamma}_5 = 2\alpha_5(\theta) \tag{4.76}$$

For a simple isotropic case:

$$p_* = \left(\frac{\partial e_{vol}}{\partial J_e}\right)_\theta = 2K(\theta)(J_e - 1) \tag{4.77}$$

$$\bar{\mathbf{S}}_* = 2\Big(\alpha_1(\theta) + \bar{I}_1\,\alpha_2(\theta)\Big)\boldsymbol{I} - 2\alpha_2(\theta)\bar{\boldsymbol{C}} = 2\alpha_1(\theta)\boldsymbol{I} + 2\alpha_2(\theta)(\bar{I}_1\,\boldsymbol{I} - \bar{\boldsymbol{C}}) \tag{4.78}$$

For pure translation $\boldsymbol{F} = \boldsymbol{I},\ \boldsymbol{C} = \bar{\boldsymbol{C}} = \boldsymbol{I},\ \bar{I}_1 = 3$

$$\begin{aligned}\bar{\mathbf{S}}_* &= \bar{\gamma}_1\,\boldsymbol{I} + \bar{\gamma}_2\,\boldsymbol{I} + \bar{\gamma}_4\,\hat{\boldsymbol{a}}_0 \otimes \hat{\boldsymbol{a}}_0 + \bar{\gamma}_5\left(\hat{\boldsymbol{a}}_0 \otimes \hat{\boldsymbol{a}}_0 + \hat{\boldsymbol{a}}_0 \otimes \hat{\boldsymbol{a}}_0\right)\\ &= \left(\bar{\gamma}_1 + \bar{\gamma}_2\right)\boldsymbol{I} + \left(\bar{\gamma}_4 + 2\bar{\gamma}_5\right)\hat{\boldsymbol{a}}_0 \otimes \hat{\boldsymbol{a}}_0\\ &= K_1\,\boldsymbol{I} + K_2\,\hat{\boldsymbol{a}}_0 \otimes \hat{\boldsymbol{a}}_0\\ &= K_1\,\boldsymbol{I} + K_2\,\boldsymbol{A}_0\end{aligned} \tag{4.79}$$

Hence,

$$\mathbf{P} : \bar{\mathbf{S}}_* = K_1 \times 0 + K_2 \times \left(\boldsymbol{A}_0 - \frac{1}{3}tr(\boldsymbol{A}_0)\boldsymbol{I}\right) = K_2 \times \left(\boldsymbol{A}_0 - \frac{1}{3}tr(\boldsymbol{A}_0)\boldsymbol{I}\right) \tag{4.80}$$

4.4. Fiber composite – viscoelastic case

The next case study pertains to composites with finite viscoelasticity. The internal energy function is assumed to be of the following form:

$$e(\theta, \boldsymbol{C}^e, \boldsymbol{\xi}_1, ..., \boldsymbol{\xi}_N) = e(\theta, \hat{\boldsymbol{a}}_0, \boldsymbol{C}^e, \boldsymbol{\xi}_1, ..., \boldsymbol{\xi}_N) \tag{4.81}$$

For the sake of brevity, let us assume that is only one internal variable for the time being, thus:

$$e(\theta, \boldsymbol{C}^e, \boldsymbol{\xi}_1, ..., \boldsymbol{\xi}_N) = e(\theta, \hat{\boldsymbol{a}}_0, \boldsymbol{C}^e, \boldsymbol{\xi}) \tag{4.82}$$

From the discussion of the previous section, it is transparent that all we need is a way to estimate the viscous stress through the internal variable. The dissipative Helmholtz potential can be written as $\psi^{visc}(\theta, \boldsymbol{\xi})$ and the evolution equation is given by:

$$\dot{\boldsymbol{\xi}} + \frac{\boldsymbol{\xi}}{\boldsymbol{\tau}} = \beta\dot{\bar{\boldsymbol{C}}}^e \tag{4.83}$$

Thereby the viscous stress is given by:

$$\boldsymbol{S}^{visc} = 2\sum \beta_\alpha \frac{\partial \psi^{visc}}{\partial \boldsymbol{\xi}_\alpha} = 2\beta \frac{\partial \psi^{visc}}{\partial \boldsymbol{\xi}} \tag{4.84}$$

A simple form of free energy that satisfies the second law dissipation inequality $\boldsymbol{S}^{visc} : \boldsymbol{\xi} \geq 0$ is given by:

$$\psi^{visc} = \frac{1}{2}\boldsymbol{\xi} : C_{visc}\boldsymbol{\xi} \tag{4.85}$$

where $\boldsymbol{C}_{visc}$ is a viscosity tensor. An easier simplification would be if it is assumed to be isotropic thereby giving:

$$\psi^{visc} = \frac{1}{2}C^{0}_{visc}\boldsymbol{\xi} : \boldsymbol{\xi} \tag{4.86}$$

Thus:

$$\boldsymbol{S}^{visc} = C^{0}_{visc}\boldsymbol{\xi} \tag{4.87}$$

For this simple case, one can write the evolution equation directly in terms of viscous stress as:

$$\dot{\boldsymbol{S}}^{visc} + \frac{\boldsymbol{S}^{visc}}{\tau} = C^{0}_{visc}\beta\dot{\bar{\boldsymbol{C}}}^{e} \tag{4.88}$$

4.5. Yarn damage mechanics

Predicting damage and progressive failure in composite materials under impact is an active area of research. The morphology of composite material induces damage accumulation before ultimate structural collapse. Hence brittle failure based criterion will not yield satisfactory results as nonlinearities induced by accumulation of damage would be stepped over. On the other hand, accounting for every crack and void nucleated during loading together with wave scattering and fiber-matrix interfacial failures through a numerical code requires the kind of resolution which is beyond the reach of current computing and imaging technology. Therefore purely computational approaches, e.g., Oskay and Fish (2007) and Belytschko et al. (2008) which need tracking of cracks explicitly with restrictions on periodicity are impractical for complex, dynamic loading of fiber reinforced composites.

Continuing from the previous grant period, we now extend the continuum damage mechanics framework to include damage mechanisms suitable for the high strain rate regime.

The total internal energy without damage can be written as:

$$e(\theta, J_e, \bar{I}_1, \bar{I}_2, \bar{I}_4, \bar{I}_5) = e_{vol}(\theta, J_e) + e_{iso}(\theta, \bar{I}_1, \bar{I}_2, \bar{I}_4, \bar{I}_5) \tag{4.89}$$

We assume that the volumetric and isochoric damages are a result of different mechanisms, with volumetric part directly contributed by pressure and the isochoric part through shear. Thus, the energy functional can be written as:

$$e = (1 - D_{vol})e_{vol}(\theta, J_e) + e_{iso}(\theta, \bar{I}_1, \bar{I}_2, \bar{I}_4, \bar{I}_5, D^1_{iso}, D^2_{iso}, D^3_{iso}, D^4_{iso}) \tag{4.90}$$

where D_{vol} and D_{iso} are the volumetric and shear damage parameters respectively. We postulate the volumetric damage evolution law as follows:

$$\dot{D}_{vol} = D_{vol}^{N_2} l_{cr}^{N_2} \left(\frac{p}{\sigma_{eq}} \right)^{N_2} \tag{4.91}$$

where N_1, N_2 and N_3 are empirical exponents, l_{cr} is the empirical characteristic flaw size, p is pressure and σ_{eq} is the von-Mises stress at the material point. The isochoric damage variables D_{iso}^1, D_{iso}^2 D_{iso}^3, D_{iso}^4 represent uniaxial tension (fiber parallel), compression (fiber perpendicular), transverse shear, and in-plane shear, respectively and each have their own evolution rules.

5. Numerical Examples

There have been relatively few experiments conducted to quantify ballistic penetration data for 3D orthogonal woven fiber composites. One of the preliminary experiments on the system currently being studied has been done by Gama et al. (2001). The authors carried out bullet impact experiments on 3D-OWC. The panels were obtained from 3Tex® Inc. In their experiments, bullets of 5 mm diameter made from Steel were fired orthogonally at these panels. The authors reported photographic evidence as well as measurements of incident and exit speeds. In this section we will simulate the event and discuss the results obtained from the model against experimental results.

5.1. Composite plate geometry

The particular three-dimensional woven fiber composite geometry considered here in constructed by repeating a fundamental unit cell, which is shown in Figure 5(a)-(c) and is developed after Chou. The overall dimensions of the unit cell are 9.236*mm* x 9.932*mm* x 5.390*mm*. The fill (X), warp (Y) and Z tows are idealized as prismatic bodies. The fiber tows are discretized using finite strain continuum shell elements and the resin by fully integrated three dimensional hexahedral elements. A minimum of four continuum shell elements are used to discretize the smallest dimension of a tow. In the overall discretization, the aspect ratios of the elements are kept similar. A total of 127616 of these continuum shell elements were used each with thickness 0.1mm and 5 integration points used for through thickness integration to model the X, Y and Z yarns. A total of 47424 of 3D fully integrated hexahederal elements were used to discretize the resin and projectile. This mesh density has been kept the same for all analysis performed in this paper.

The plate is clamped at the boundaries allowing for no slip at the clamps. Furthermore, symmetry boundary conditions are used to model only quarter of a plate and hence 4 repeating unit cells as our computational domain can be used to model a plate 4 times as large.

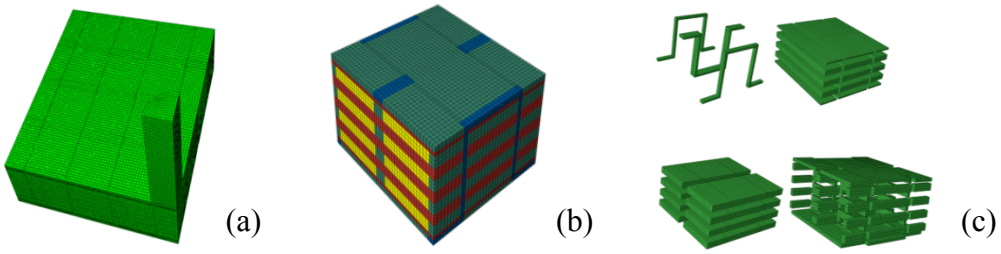

Figure 5: (a) Impact system setup with a quarter plate and quarter of a rigid right cylindrical projectile (b) unit cell (c) meso scale components making up the unit cell.

Since we are interested in investigating penetration, a sufficiently high enough projectile speed will be taken. Penetration is a complex process and depends on a large number of parameters. Projectile momentum as well as mechanical properties determine the time of penetration. At high speed penetration boundary conditions are of little significance due to highly localized damage. In this section we present some numerical examples of simulations of projectile impact at 500 *m/s* on a three dimensional woven fiber composite plate. The projectile is assumed to be a rigid right circular cylinder under isothermal conditions with mass of 1 *gram* and diameter of 5*mm* to represent the projectile used in the ballistic experiment.

5.2. Experimental validation and key insights

5.2.1. Hyperbolic damage profile

The damaged zone which corresponds to the region of high stress transients has a hyperbolic front centered at the point of impact. Clearly the evolving stress contours in Figure 6(c) indicate an advancing hyperbolic stress front. Our simulations from Figure 6 clearly reproduce the characteristic diamond shaped failure region at the front and at the back as observed in the experiments. Our simulations also show localized Z-fiber damage as reported by the experiments (Gama 2001).

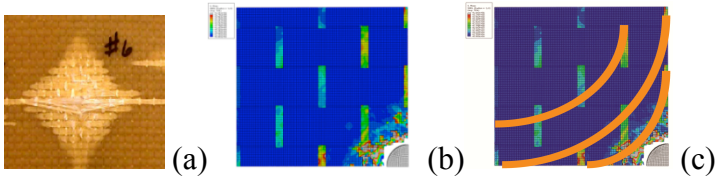

Figure 6: (a) Experimental photographs of plate rear side by Gama et al. (2001); (b) qualitative comparison of simulation results with experiments done by Gama et al. (2001) (c) hyperbolic profile of the advancing stress front.

5.2.2. Highly Directional Rear Face Tensile Damage Distribution

The next figure shows the spatial distribution of the tensile damage field of the rear face just after a perforation event has taken place. In the experimental results, there is a marked difference in the damage directionality of the strike face compared to the rear face as seen in Figure 7(a).

The Figure 7(b) corroborates the fact. The directionality is defined with respect to the direction of Z fiber windings over the matrix.

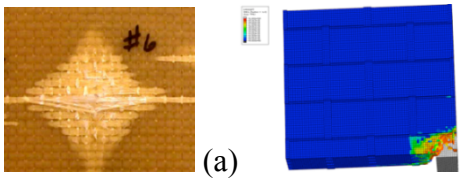

(a) (b)

Figure 7: (a) Tensile damage region just after penetration (b) fiber damage and pullout visible in experiments done by Gama et al. (2001).

5.2.3. Bulk Matrix Rate Effects Show Two Distinct Regimes

Disappearance of rate effects (Figure 8(a)-(b)) is very interesting as, theoretically, rate effects should be minimal for quasi-static indentation and maximum for high speed impacts. We explain this apparent paradox by realizing that as the matrix resin stiffens at high strain rates, there is a competing nonlinearity due to the onset of damage. Hence, corresponding to a high speed impact, the improvement in ballistic resistance due to rate effects is effectively nullified by a rapid onset of material failure. This anomaly of diminishing rate effects have been observed by before during the shock plate experiments of (Pankow et al. 2011) and cannot be explained by hot-spot analysis only without incorporating a damage law into the formulation.

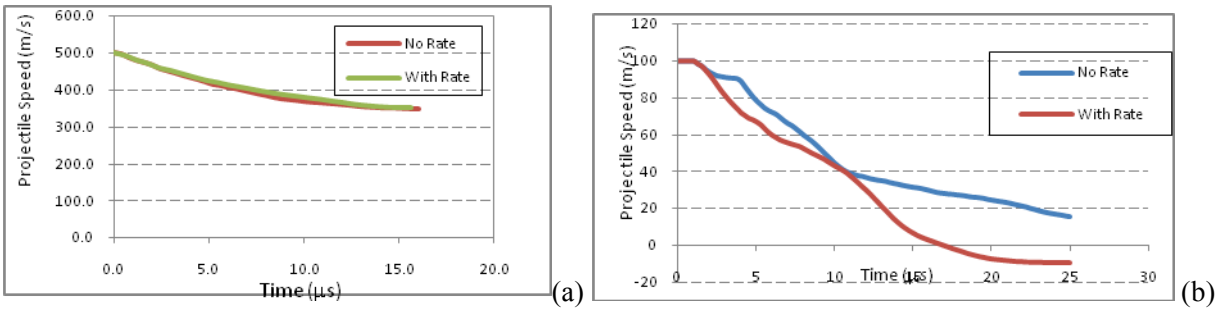

(a) (b)

Figure 8 (a) Projectile velocity-time profile comparison between models with and without rate effects at 500*m/s* (b) Projectile velocity comparison between models with and without rate effects at 100*m/s*

5.2.4. Damage Anisotropy Effect of Z-fiber on Matrix and Fiber Damage

The effect of Z-fibers is more than simply preventing delamination across inter-ply layers. Figure 9(a) shows that the Z-fibers running on the surface of the Y-fibers in an orthogonal direction scatter the stress waves away from them, thereby reducing the immediate area of damage. The damage is thus restricted primarily in the Y-direction. Z-fibers thus cause directional damage in the fibers but diffuse damage in the matrix in the yarns. Figure 9(a), (c) and (b), (d) show the fiber compression and tensile damage damage in 3D-OWC and 2D layered composites, respectively. The left and right panels of Figure 10(a)-(f) show that in spite of highly localized terminal the matrix damage at Z fiber sites has potential for void growth and interlaminar cracks thereby reducing the ability of Z-fibers to act effectively during future impact events. Clearly the purported benefits of Z fibers over stitched composites are that it doesn't physically damage the

composite structure. In deed this conclusion has been experimentally observed by Pankow et al. (2011) during shock loading of these panels who noted that beyond 6% Z-fiber concentration, the stiffness properties appreciably deteriorate.

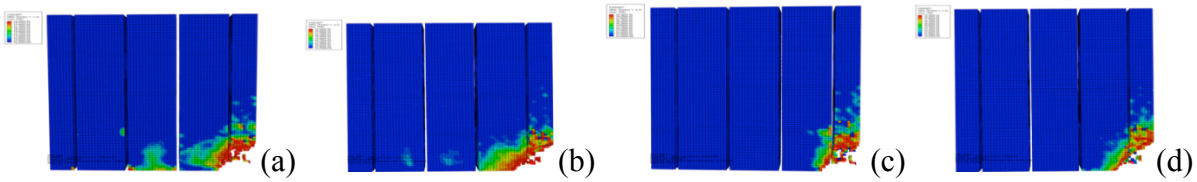

Figure 9: (a): Strike face fiber tension damage for 3D OWC (b) Strike face fiber tension damage for layered composite (c) Strike face fiber compression damage for 3D OWC (d) Strike face fiber compression damage for layered composite

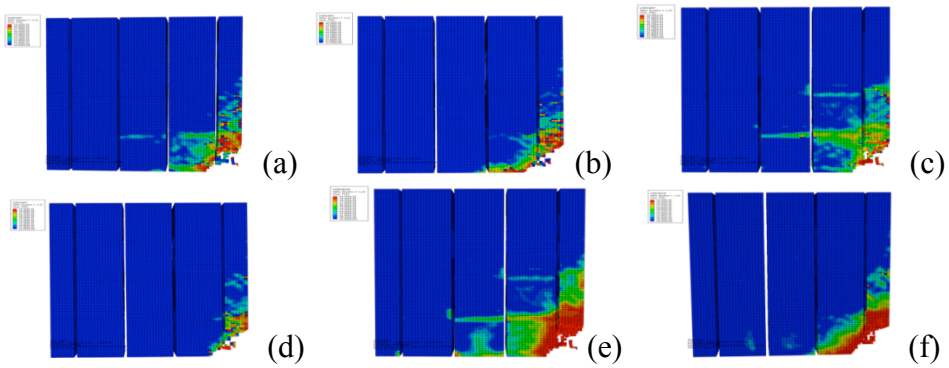

Figure 10: (a): Strike face fiber tension damage for 3D OWC (b) Strike face fiber tension damage for layered composite (c) Strike face fiber compression damage for 3D OWC (d) Strike face fiber compression damage for layered composite

Finally, Table 6 gives the summary of the challenges and achievements for the macro-scale modeling.

Table 6: Summary of challenges and their resolution

Modeling and Computational Challenges	Successful Resolution
Damage laws	Meso level micromechanics
Damage initiation rate sensitivity	Modified Hashin
Resin ductile to brittle transition	Terminal thermo-mechanical damage law
Damage evolution	Crack band type regularized fracture mechanics based model

5.3. Study of anisotropic composite material response with changing material parameter

We now examine the effect of Gruneisen tensor on the composite materials response. The Gruneisen parameter is an important material property quantifying the entropy dependence on deformation for a material. In a typical shock physics application (Davison 2008), this is treated

as a scalar variable. This is justified through the reasoning that shock regime comprises of bulk response of a material which is well past the shear limit of a typical material. In our computational material model, we found that for anisotropic materials, the full tensorial representation is critical to capture the essential physics of the process. In the Figure 11 and 12, we show that varying the anisotropy of Gruneisen tensor can have significant impact on the incipient plasticity of a material. We show that as this tensor is rotated about [100] (Figure 11) and [001] (Figure 12), the J_2 changes significantly even though the bulk response may not. We also report that even in the case of isotropic solids with anisotropic Gruneisen tensor, same effects show up.

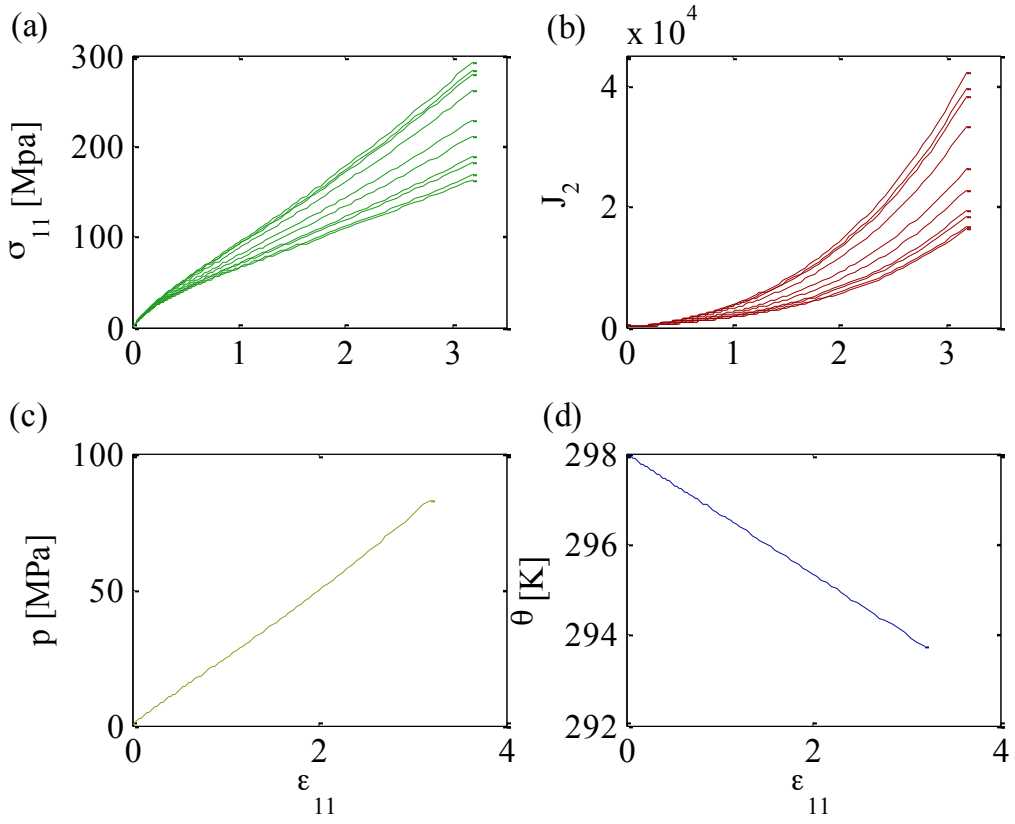

Figure 11: Anisotropic material response with changing Gruneisen tensor (rotation about [100]).

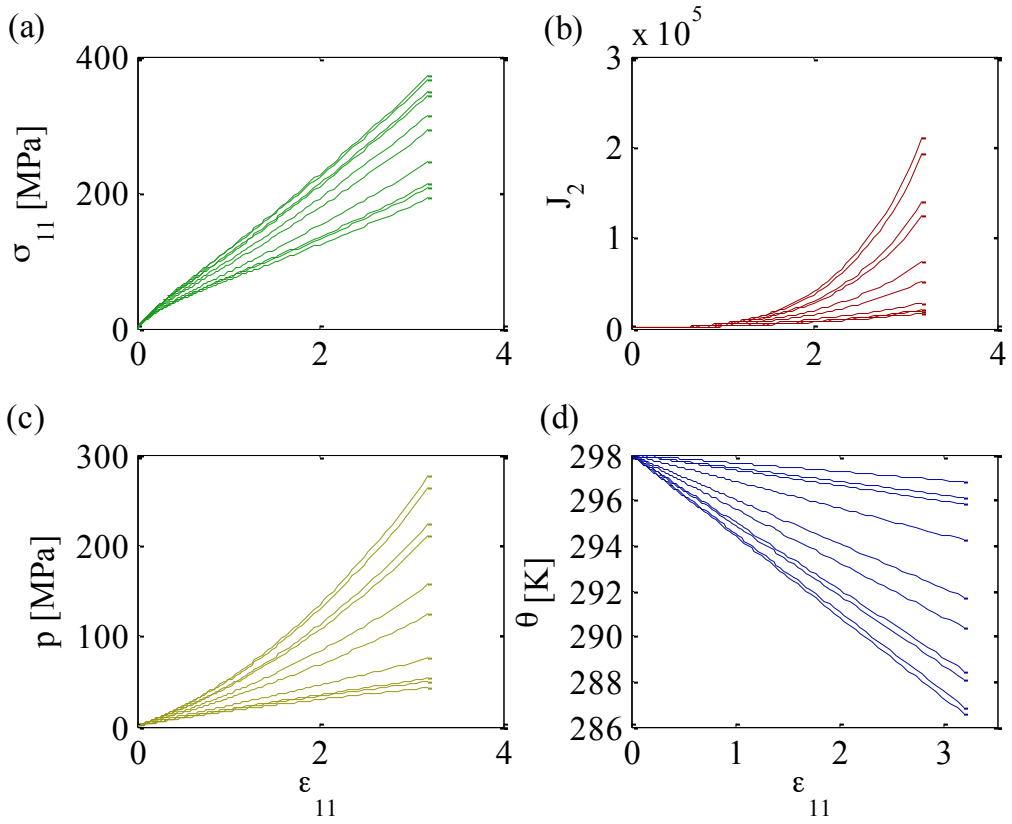

Figure 12: Anisotropic material response with changing Gruneisen tensor (rotation about [001]).

6. Summary

We achieved or even exceeded key goals to achieve a multiscale damage model for the impact problem proposed. The meso scale damage mechanics avoids the theoretical pitfalls associated with regular multiscale methods based on fiber level classical homogenization as well as unit cell level averaging methods. The anisotropic yarn properties are modeled using generalized self-consistent method for fiber composites. This method has the advantage of yielding closed form expressions. The model predicted various experimental observations from direct penetration tests as well as standardized split Hopkinson and shock plate impact tests as well. We found that both Z-fiber and bulk matrix rate effects can improve ballistic resistance depending on the momentum of the projectile and dimension of the plate. However, in the penetration range, competing nonlinearities tend to nullify each other producing both localized effects and potential crack nucleation sites through wave propagation. We also found that the effect of Z–fiber on damage distribution is not straightforward and analysis of both fiber and matrix damage mode explained many of the unique damage features of 3D-OWC. Although obtaining data for fitting damage models remains, we have drastically cut the number of arbitrary parameters necessary to obtain predictive capabilities. This model of the yarn is further extended into a large deformation model. We propose a damage law based on consistent thermomechanics for a typical

unidirectional composite, which can be easily extended for composites with greater degree of anisotropy. We examined the effect of material parameter such as Gruneisen tensor on the composite materials response. In our computational material model, we found that for anisotropic materials, the full tensorial representation is critical to capture the essential physics of the process. We also report that even in the case of isotropic solids with anisotropic Gruneisen tensor, same effects show up. However, we could not validate our model due to lack to experimental data. Overall, this mesoscale model while less computationally expensive than a standard homogenization, it still remains computationally prohibitive for large plate impacts. The next step in addition to parameter estimation would be to develop a continuum level model to make the model amenable to large-scale computations.

7. Bibliography

Abeysinghe, Tilak. 2001. "Estimation of direct and indirect impact of oil price on growth." *Economics Letters* 73 (2) (November): 147-153. doi:doi: 10.1016/S0165-1765(01)00476-1.

Anderson, C. E., P. E. O'Donoghue and D. Skerhut. 1990. "A Mixture Theory Approach for the Shock Response of Composite Materials." *J. Composite Materials,* 24:1160-1178.

Anderson, C. E., P. A. Cox, G. R. Johnson and P. J. Maudlin. 1994. "A Constitutive Formulation for Anisotropie Materials Suitable for Wave Propagation Computer Programs-II" *Computational Mechanics,* 15:201-223.

Bažant, Zdeněk P., and B. H. Oh. 1983. "Crack band theory for fracture of concrete." *Matériaux et Constructions* 16 (3): 155-177. doi:10.1007/BF02486267.

Baheieldin, Y, A. M. Rajendran, and M. A. Zikry. 2004. "A micromechanical model for damage progression in woven composite systems." *International Journal of Solids and Structures* 41 (9-10): 2307-2330. doi:10.1016/j.ijsolstr.2003.12.006.

Bahei-El-Din, Y, and Mohammed A. Zikry. 2003. "Impact-induced deformation fields in 2D and 3D woven composites." *Composites Science and Technology* 63 (7): 923-942. doi:10.1016/S0266-3538(03)00021-6.

Belytschko, Ted, Stefan Loehnert, and Jeong-Hoon Song. 2008. "Multiscale aggregating discontinuities: A method for circumventing loss of material stability." *International Journal for Numerical Methods in Engineering* 73 (6): 869-894. doi:10.1002/nme.2156.

Bergström, J. S., C. M. Rimnac, and S. M. Kurtz. 2005. "Molecular chain stretch is a multiaxial failure criterion for conventional and highly crosslinked UHMWPE." *Journal of Orthopaedic Research* 23 (2): 367-375. doi:10.1016/j.orthres.2004.08.014.

Boyce, M, D Parks, and A Argon. 1988. "Large inelastic deformation of glassy polymers. part I: rate dependent constitutive model." *Mechanics of Materials* 7 (1): 15-33. doi:10.1016/0167-6636(88)90003-8.

Christensen, R. 1990. "A critical evaluation for a class of micro-mechanics models." *Journal of the Mechanics and Physics of Solids* 38 (3): 379-404. doi:10.1016/0022-5096(90)90005-O.

Davison L. *Fundamentals of shockwave propagation in solids*. Berlin: Springer-Verlag; 2008.

Dow Epoxy Values. http://epoxy.dow.com/epoxy/products/prod/intermed.htm.

Gama, B. 2001. "Ballistic impact damage modeling and experimental validation on a 3-D orthogonal weave fabric composite ." *Proceedings of SAMPE 2005.*

Garg, M., AD Mulliken, and MC Boyce. 2008. “Temperature Rise in Polymeric Materials During High Rate Deformation.” *Journal of Applied Mechanics* 75 (1): 011009. doi:10.1115/1.2745388.

Greenhalgh, Emile. 2009. *Failure analysis and fractography of polymer composites*. Cambridge UK ;Boca Raton FL: Woodhead Publishing ;;CRC Press.

Hahn, H. T., and S. W. Tsai. 1973. “Nonlinear Elastic Behavior of Unidirectional Composite Laminae.” *Journal of Composite Materials* 7 (1): 102-118. doi:10.1177/002199837300700108.

Hashin, Z., and A. Rotem. 1973. “A Fatigue Failure Criterion for Fiber Reinforced Materials.” *Journal of Composite Materials* 7 (4): 448-464. doi:10.1177/002199837300700404.

Jordan, Jennifer L., Jason R. Foley, and Clive R. Siviour. 2008. “Mechanical properties of Epon 826/DEA epoxy.” *Mechanics of Time-Dependent Materials* 12 (3): 249-272. doi:10.1007/s11043-008-9061-x.

Lapczyk, I, and J Hurtado. 2007. “Progressive damage modeling in fiber-reinforced materials.” *Composites Part A: Applied Science and Manufacturing* 38 (11): 2333-2341. doi:10.1016/j.compositesa.2007.01.017.

Leigh Phoenix, S, and Pankaj K Porwal. 2003. “A new membrane model for the ballistic impact response and V50 performance of multi-ply fibrous systems.” *International Journal of Solids and Structures* 40 (24): 6723-6765. doi:10.1016/S0020-7683(03)00329-9.

Lemaître, J. 2005. *Engineering damage mechanics : ductile, creep, fatigue and brittle failures*. Berlin ;;New York: Springer.

Matzenmiller, A. 1995. “A constitutive model for anisotropic damage in fiber-composites.” *Mechanics of Materials* 20 (2): 125-152. doi:10.1016/0167-6636(94)00053-0.

Meyers, Marc. 1994. *Dynamic behavior of materials*. New York: Wiley.

Mulliken, A, and M Boyce. 2006. “Mechanics of the rate-dependent elastic–plastic deformation of glassy polymers from low to high strain rates.” *International Journal of Solids and Structures* 43 (5): 1331-1356. doi:10.1016/j.ijsolstr.2005.04.016.

Nadler, Ben, Panayiotis Papadopoulos, and David J. Steigmann. 2006. “Multiscale constitutive modeling and numerical simulation of fabric material.” *International Journal of Solids and Structures* 43 (2): 206-221. doi:10.1016/j.ijsolstr.2005.05.020.

Nemat-Nasser, S. 1993. *Micromechanics : overall properties of heterogeneous materials*. Amsterdam ;;New York: North-Holland.

Oskay, C, and J Fish. 2007. “Eigendeformation-based reduced order homogenization for failure analysis of heterogeneous materials.” *Computer Methods in Applied Mechanics and Engineering* 196 (7): 1216-1243. doi:10.1016/j.cma.2006.08.015.

Pankow, M., B. Justusson, A. Salvi, A.M. Waas, C-F Yen, and Seth Ghiorse. 2011. “Shock response of 3D woven composites: An experimental investigation.” *Composite Structures* 93 (5): 1337-1346. doi:10.1016/j.compstruct.2010.10.021.

Pankow, M., A. Salvi, A.M. Waas, CF Yen, and S. Ghiorse. 2011. “Split Hopkinson pressure bar testing of 3D woven composites.” *Composites Science and Technology* 71 (9): 1196-1208. doi:10.1016/j.compscitech.2011.03.017.

Pankow, M., A.M. Waas, C-F Yen, and Seth Ghiorse. 2011. “Shock loading of 3D woven composites: A validated finite element investigation.” *Composite Structures* 93 (5): 1347-1362. doi:10.1016/j.compstruct.2010.11.001.

Parhizgar, Shahrokh, Loren W. Zachary, and CT Sun. 1982. “Application of the principles of linear fracture mechanics to the composite materials.” *International Journal of Fracture* 20 (1): 3-15. doi:10.1007/BF00942161.

Pinho, S, P Robinson, and L Iannucci. 2006. “Fracture toughness of the tensile and compressive fibre failure modes in laminated composites.” *Composites Science and Technology* 66 (13): 2069-2079. doi:10.1016/j.compscitech.2005.12.023.

Simo, J. C. 1987. “On a fully three-dimensional finite-strain viscoelastic damage model: Formulation and computational aspects”, *Computer Methods in Applied Mechanics and Engineering* 60(2): 153-173. doi: 10.1016/0045-7825(87)90107-1.

Sun, B, Yuankun Liu, and Bohong Gu. 2009. “A unit cell approach of finite element calculation of ballistic impact damage of 3-D orthogonal woven composite.” *Composites Part B: Engineering* 40 (6): 552-560. doi:10.1016/j.compositesb.2009.01.012.

Walter, T.R., G. Subhash, B.V. Sankar, and CF Yen. 2009. “Damage modes in 3D glass fiber epoxy woven composites under high rate of impact loading.” *Composites Part B: Engineering* 40 (6): 584-589. doi:10.1016/j.compositesb.2009.04.021.

Xiwen Jia, Baozhong Sun, , and , Bohong Gu. 2010. “Ballistic penetration of conically cylindrical steel projectile into 3D orthogonal woven composite: a finite element study at microstructure level.” *Journal of Composite Materials* 45 (9): 965-987. doi:10.1177/0021998310381150.